ORTA DOĞU TEKNİK ÜNİVERSİTESİ
FEN BİLİMLERİ ENSTİTÜSÜ MÜDÜRLÜĞÜ

TEZ ŞABLONU ONAY FORMU
THESIS TEMPLATE CONFIRMATION FORM

1. Şablonda verilen yerleşim ve boşluklar değiştirilmemelidir.
2. **Jüri tarihi** Başlık Sayfası, İmza Sayfası, Abstract ve Öz'de ilgili yerlere yazılmalıdır.
3. İmza sayfasında jüri üyelerinin unvanları doğru olarak yazılmalıdır. Tüm imzalar **mavi pilot kalemle** atılmalıdır.
4. **Disiplinlerarası** programlarda görevlendirilen öğretim üyeleri için jüri üyeleri kısmında tam zamanlı olarak çalıştıkları anabilim dalı başkanlığının ismi yazılmalıdır. Örneğin: bir öğretim üyesi Biyoteknoloji programında görev yapıyor ve biyoloji bölümünde tam zamanlı çalışıyorsa, İmza sayfasına biyoloji bölümü yazılmalıdır. İstisnai olarak, disiplinler arası program başkanı ve tez danışmanı için disiplinlerarası program adı yazılmalıdır.
5. Tezin **son sayfasının sayfa** numarası Abstract ve Öz'de ilgili yerlere yazılmalıdır.
6. Bütün chapterlar, referanslar, ekler ve CV sağ sayfada başlamalıdır. Bunun için **kesmeler** kullanılmıştır. **Kesmelerin kayması** fazladan boş sayfaların oluşmasına sebep olabilir. Bu gibi durumlarda paragraf (¶) işaretine tıklayarak kesmeleri görünür hale getirin ve yerlerini **kontrol edin**.
7. Figürler ve tablolar kenar boşluklarına taşmamalıdır.
8. Şablonda yorum olarak eklenen uyarılar dikkatle okunmalı ve uygulanmalıdır.
9. Tez yazdırılmadan önce PDF olarak kaydedilmelidir. Şablonda yorum olarak eklenen uyarılar PDF dokümanında yer almamalıdır.
10. Tez taslaklarının kontrol işlemleri tamamlandığında, bu durum öğrencilere METU uzantılı öğrenci e-posta adresleri aracılığıyla duyurulacaktır.
11. Tez yazım süreci ile ilgili herhangi bir sıkıntı yaşarsanız, Sıkça Sorulan Sorular (SSS) sayfamızı ziyaret ederek yaşadığınız sıkıntıyla ilgili bir çözüm bulabilirsiniz.

1. Do not change the spacing and placement in the template.
2. Write **defense date** to the related places given on Title page, Approval page, Abstract and Öz.
3. Write the titles of the examining committee members correctly on Approval Page. **Blue ink** must be used for all signatures.
4. For faculty members working in **interdisciplinary programs**, the name of the department that they work full-time should be written on the Approval page. For example, if a faculty member staffs in the biotechnology program and works full-time in the biology department, the department of biology should be written on the approval page. Exceptionally, for the interdisciplinary program chair and your thesis supervisor, the interdisciplinary program name should be written.
5. Write **the page number of the last page** in the related places given on Abstract and Öz pages.
6. All chapters, references, appendices and CV must be started on the right page. **Section Breaks** were used for this. **Change in the placement** of section breaks can result in extra blank pages. In such cases, make the section breaks visible by clicking paragraph (¶) mark and **check their position.**
7. All figures and tables must be given inside the page. Nothing must appear in the margins.
8. All the warnings given on the comments section through the thesis template must be read and applied.
9. Save your thesis as pdf and Disable all the comments before taking the printout.
10. This will be announced to the students via their METU students e-mail addresses when the control of the thesis drafts has been completed.
11. If you have any problems with the thesis writing process, you may visit our Frequently Asked Questions (FAQ) page and find a solution to your problem.

☒ **Yukarıda bulunan tüm maddeleri okudum, anladım ve kabul ediyorum. / I have read, understand and accept all of the items above.**

Name : Seher
Surname : Topuz
E-Mail : seher.topuz@metu.edu.tr
Date :
Signature : _____

EFFECT OF ALLOYING ELEMENTS AND HEAT TREATMENT ON FATIGUE CRACK GROWTH BEHAVIOR OF FE-NI-BASED SUPERALLOYS

A THESIS SUBMITTED TO
THE GRADUATE SCHOOL OF NATURAL AND APPLIED SCIENCES
OF
MIDDLE EAST TECHNICAL UNIVERSITY

BY

SEHER TOPUZ

IN PARTIAL FULFILLMENT OF THE REQUIREMENTS
FOR
THE DEGREE OF MASTER OF SCIENCE
IN
METALLURGICAL AND MATERIALS ENGINEERING

DECEMBER 2022

Approval of the thesis:

EFFECT OF ALLOYING ELEMENTS AND HEAT TREATMENT ON FATIGUE CRACK GROWTH BEHAVIOR OF FE-NI-BASED SUPERALLOYS

submitted by **SEHER TOPUZ** in partial fulfillment of the requirements for the degree of **Master of Science** i**n Metallurgical and Materials Engineering, Middle East Technical University** by,

Prof. Dr. Halil Kalıpçılar
Dean, Graduate School of **Natural and Applied Sciences** _____

Prof. Dr. Ali Kalkanlı
Head of the Department, **Metallurgical and Materials Eng.** _____

Prof. Dr. Rıza Gürbüz
Supervisor, **Metallurgical and Materials Eng., METU** _____

Dr. Caner Batıgün
Co-Supervisor, **Metallurgical and Materials Eng., METU** _____

Examining Committee Members:

Prof. Dr. Bilgehan Ögel
Metallurgical and Materials Eng, METU _____

Prof. Dr. Rıza Gürbüz
Metallurgical and Materials Eng, METU _____

Prof. Dr. Ziya Esen
Materials Science and Eng, Çankaya University _____

Assoc. Prof. Caner Şimşir
Metallurgical and Materials Eng, METU _____

Assist. Prof. Dr. Bilge İmer
Metallurgical and Materials Eng, METU _____

Date: 02.12.2022

I hereby declare that all information in this document has been obtained and presented in accordance with academic rules and ethical conduct. I also declare that, as required by these rules and conduct, I have fully cited and referenced all material and results that are not original to this work.

Name Last name: Seher Topuz

Signature:

ABSTRACT

EFFECT OF ALLOYING ELEMENTS AND HEAT TREATMENT ON FATIGUE CRACK GROWTH BEHAVIOR OF FE-NI-BASED SUPERALLOYS

Topuz, Seher
Master of Science, Metallurgical and Materials Engineering
Supervisor: Prof. Dr. Rıza Gürbüz
Co-Supervisor: Dr. Caner Batıgün

December 2022, 76 pages

Fe-Ni-based superalloys are characterized by high strength, toughness, and corrosion resistance materials at room and elevated temperature applications. They are generally used in many parts requiring high toughness and ductility, such as aerospace, industrial gas turbine, and industrial components. The mechanical properties of Fe-Ni-based superalloys depend on three main effects. These alloying elements are added to the structure, working processes, and heat treatment. This study investigates the effect of alloying elements after heat treatment on the characterization and fatigue crack growth behavior of three Fe-Ni-based superalloys with different compositions. The results show that Fe-Ni-based superalloys with different chemical compositions and production routines give different heat treatment mechanisms respond to the same heat treatment parameters. Also, the effect of γ' formation and carbide precipitation are discussed on the mechanical properties of different Fe-Ni-based superalloys with heat treatment.

Keywords: Fe-Ni based superalloy, heat treatment, fatigue crack growth, alloying elements

ÖZ

ALAŞIM ELEMENTLERİ VE ISIL İŞLEMİN FE-Nİ ESASLI SÜPERALAŞIMLARIN YORULMA ÇATLAĞI İLERLEMESİ TAVRI ÜZERİNDEKİ ETKİSİ

Topuz, Seher
Yüksek Lisans, Metalurji ve Malzeme Mühendisliği
Tez Yöneticisi: Prof. Dr. Rıza Gürbüz
Ortak Tez Yöneticisi: Dr. Caner Batıgün

Aralık 2022, 76 sayfa

Fe-Ni esaslı süperalaşımlar oda sıcaklığında ve yüksek sıcaklık değerlerinde mukavemeti, tokluğu ve korozyon direnci yüksek malzemeler olarak tanımlanırlar. Bu süperalaşımlar tokluğun ve sünekliğin önemli olduğu havacılık, gaz tübini ve sanayide bulunan birçok parçada yaygın olarak kullanılmaktadırlar. Fe-Ni esaslı süper alaşımların mekanik özellikleri direkt olarak yapısında bulunan alaşım elementlerinin yanı üretim yöntemine ve ısıl işleme bağlıdır. Bu çalışmada 3 farklı kompozisyona sahip Fe-Ni esaslı süperalaşımda ısıl işlem sonrası alaşım elementlerinin karakterizasyon ve yorulma çatlağı ilerlemesi üzerindeki etkisi incelenmiştir. Çalışma sonuçlarına göre, farklı kimyasal kompozisyona ve üretim yöntemine sahip Fe-Ni esaslı süperalaşımların aynı ısıl işlem parametresine farklı cevaplar verdiği görülmüştür. Buna ek olarak, ısıl işlem sonrası γ’ oluşumu ve karbürlerin mekanik özellikler üzerindeki etkisi değerlendirilmiştir.

Anahtar Kelimeler: Fe-Ni esaslı süperalaşım, ısıl işlem, yorulma çatlağı ilerlemesi, alaşım element

To My Mom, Dad, and Nil Eylül

ACKNOWLEDGMENTS

I wish to express my deepest gratitude to my supervisor, Prof. Dr. Rıza Gürbüz and co-supervisor Dr. Caner Batıgün for their guidance, advice, and encouragements throughout the research.

I would also like to thank Dr. Ali Motemeni and Servet Şehirli for their suggestions comments and helps in this research.

I owe special thanks to Tuğba Ölmez and Derin Machining family, Yusuf Yıldırım, Cemal Yanardağ, Önder Şahin, and Onur Yıldırım for their help during the preparation of samples and tests.

I also special thank firm Onatus for the JmatPro analysis. I am also grateful to the first school of my business life Döksan Heat Treatment Company, and Gürkan Gençler for their support, understanding and learning. I would like to extend my sincere thanks to Çelebi Ersoy for his support.

I would like to express my deepest appreciation to Ali Emre Tanrısevdi and Ezgi Bengü Durak for their support throughout the master thesis.

My friends Dilara, Beste, Nasiye, Şule, Ebru, Gökhan, Gizem, Meysun, Ayça, Çağlar, Burak, Dere, Koray, Fevziye, Gözde, Yasin, Erdi, and Abdullah are always appreciated for their support, encouragement and believe in me.

I am also grateful to my big family, my grandfathers Ahmet and Haydar, my grandmothers Zülfiye and Gülhanım, My uncles Hüseyin, Muharrem and Serdar, My dearest aunt İmren and Mehtap, brother in law Müslüm, Köksal, İbrahim, and Hüseyin, aunt in law Elif and Çağla, my secondary aunts Meray and Kibar and my cousins for their support and love in my whole life.

Finally, I cannot thank enough my mom, dad, and sister for their understanding, help, patience, and empathy.

TABLE OF CONTENTS

ABSTRACT v

ÖZ vi

ACKNOWLEDGMENTS viii

TABLE OF CONTENTS ix

LIST OF TABLES xi

LIST OF FIGURES xii

LIST OF ABBREVIATIONS xvi

1 INTRODUCTION 1

1.1 Motivation 1

2 LITERATURE REVIEW 3

2.1 General Information About Superalloys 3

2.2 Types of Superalloys 4

2.2.1 Ni-Based Superalloys 5

2.2.2 Co-Based Superalloys 6

2.2.3 Fe-Ni Based Superalloys 6

2.3 Heat Treatment of Fe-Ni-Based Superalloys 10

2.3.1 Heat Treatment Types for Fe-Ni-Based Superalloy 10

2.3.2 Strengthening for Fe-Ni-Based Superalloy 11

2.3.3 Effect of Solution Heat Treatment and Aging on Microstructure and Mechanical Properties of Fe-Ni-Based Superalloys 12

3 EXPERIMENTAL PROCEDURE 17
3.1 Materials Used in Experiments 17
3.2 Heat Treatment 18
3.3 Characterization Tests 20
3.3.1 Hardness Test 20
3.3.2 Spectral Analysis 21
3.3.3 Microstructural Analysis 22
3.3.4 Tensile Test 25
3.4 Fatigue Crack Growth Rate Test 27
4 RESULTS & DISCUSSION 33
4.1 Material Characterization Results 33
4.1.1 Chemical Composition Analysis Results 33
4.1.2 Hardness Test Results 34
4.1.3 Tensile Test Results 36
4.1.4 Optical Microscope Results 40
4.1.5 SEM Analysis Results of Microstructure 48
4.1.6 Fatigue Crack Growth Test Results 55
4.1.7 Fractographic Results 65
5 CONCLUSION 71
REFERENCES 73

LIST OF TABLES

TABLES

Table 1. Effects of elements in Fe-Ni-based superalloys [2] 8
Table 2. Phases in Fe-Ni-based superalloys [13] 9
Table 3. Numerical name of all samples 17
Table 4. Test load and frequency parameters 30
Table 5. Chemical compositions of three different samples 33
Table 6. Mechanical properties of test samples 38
Table 7. m, C, R^2, near ΔK_{th} and ΔK_{max} values of test samples 62

LIST OF FIGURES

FIGURES

Figure 1. Creep strength and oxidation resistance of some materials with temperature [3] 3
Figure 2. Crystal structures in superalloys [2] 5
Figure 3. Schematic representation of the microstructure of Fe-Ni-based superalloys 12
Figure 4. a-N curve [25] 14
Figure 5. da/dN versus ΔK curves for fatigue crack growth [26] 15
Figure 6. Heat treatment steps of Fe-Ni-based superalloys 18
Figure 7. Solution heat treatment furnace 19
Figure 8. Aging heat treatment furnace 19
Figure 9. All samples in the furnace for solution heat treatment and aging 20
Figure 10. Micro vickers hardness tester 21
Figure 11. Spectroscopy analyzer 22
Figure 12. Abrasive cutter 22
Figure 13. Bakelite machine 23
Figure 14. Grinder 23
Figure 15. Polisher 24
Figure 16. Optical microscope 25
Figure 17. Tensile test specimen dimensions [28] 26
Figure 18. Tensile test machine 26
Figure 19. Fatigue crack growth test specimen dimensions [29] 27
Figure 20. Fatigue crack growth sample production dimensions [29] 27
Figure 21. Universal fatigue crack growth machine 28
Figure 22. Fatigue crack growth sample and drawn lines 28
Figure 23. Fatigue crack growth samples from test 29
Figure 24. Loading during fatigue crack growth test 29
Figure 25. Crack growth test setup 31

Figure 26. Hardness results of 100 (as received) and 100H (as heat treated)..... 34
Figure 27. Hardness results of 200 (as received) and 200H (as heat treated)..... 34
Figure 28. Hardness results of 300 (as received) and 300H (as heat treated)..... 35
Figure 29. Hardness results of 100, 200, and 300 (as received) 35
Figure 30. Hardness results of 100H, 200H, and 300H (as heat treated) 36
Figure 31. Tensile test results of 100 (as received) and 100H (as heat treated) 37
Figure 32. Tensile test results of 200 (as received) and 200H (as heat treated) 37
Figure 33. Tensile test results of 300 (as received) and 300H (as heat treated) 37
Figure 34. Tensile test results of 100, 200, and 300 (as received)..... 39
Figure 35. Tensile test results of 100H, 200H, and 300H (as heat treated) 39
Figure 36. 100 (as received) at 100x magnification..... 40
Figure 37. 100H (as heat treated) at 100x magnification..... 40
Figure 38. 100 (as received) at 200x magnification..... 41
Figure 39. 100H (as heat treated) at 200x magnification..... 41
Figure 40. 100 (as received) at 500x magnification..... 42
Figure 41. 100H (as heat treated) at 500x magnification..... 42
Figure 42. 200 (as received) at 100x magnification..... 43
Figure 43. 200H (as heat treated) at 100x magnification..... 43
Figure 44. 200 (as received) at 200x magnification..... 43
Figure 45. 200H (as heat treated) at 200x magnification..... 44
Figure 46. 200 (as received) at 500x magnification..... 44
Figure 47. 200H (as heat treated) at 500x magnification..... 44
Figure 48. 300 (as received) at 100x magnification..... 45
Figure 49. 300H (as heat treated) at 100x magnification..... 45
Figure 50. 300 (as received) at 200x magnification..... 46
Figure 51. 300H (as heat treated) at 200x magnification..... 46
Figure 52. 300 (as received) at 500x magnification..... 46
Figure 53. 300H (as heat treated) at 500x magnification..... 47
Figure 54. SEM analysis results of 100 48

Figure 55. SEM results for 100 at higher magnification and EDS analysis of matrix 48
Figure 56. SEM analysis result of 100H general (left) and grain boundary (right) detailed view 49
Figure 57. SEM and EDS analysis result of dark (left) and light (right) matrix of 100H 49
Figure 58. SEM and EDS analysis of grain boundary of 100H 50
Figure 59. SEM and EDS analysis of 200 51
Figure 60. SEM (above) and EDS analysis (below) on cubic particles of 200H 52
Figure 61. CCT and TTT Diagram for 100 with JMatPro Analysis 53
Figure 62. Phase formation after heat treatment for 100 53
Figure 63. CCT and TTT Diagram for 200 with JMatPro Analysis 53
Figure 64. Phase formation after heat treatment for 200 54
Figure 65. CCT and TTT Diagram for 300 with JMatPro Analysis 54
Figure 66. Phase formation after heat treatment for 300 54
Figure 67. a-N diagram of 100 and 100H 55
Figure 68. a-N diagram of 200 and 200H 56
Figure 69. a-N diagram of 300 and 300H 56
Figure 70. a-N graph with trend line for 100 and 100H 57
Figure 71. a-N graph with trend line for 200 and 200H 57
Figure 72. a-N graph with trend line for 300 and 300H 58
Figure 73. da/dN- ΔK graph of 100 59
Figure 74. da/dN- ΔK graph of 100H 60
Figure 75. da/dN- ΔK graph of 200 60
Figure 76. da/dN- ΔK graph of 200H 61
Figure 77. da/dN- ΔK graph of 300 61
Figure 78. da/dN- ΔK graph of 300H 62
Figure 79. da/dN- ΔK graph of 100 and 100H 63
Figure 80. da/dN- ΔK graph of 200 and 200H 63
Figure 81. da/dN- ΔK graph of 300 and 300H 64

Figure 82. Tensile fracture surface of 100 at SEM and EDS analysis of cubic particle..... 65
Figure 83.Tensile fracture surface of 100H at SEM 66
Figure 84. Tensile fracture surface of 200 (left) and 200H (right) at SEM 66
Figure 85. Tensile fracture surface of 300 (left) and 300H (right) at SEM 66
Figure 86. Fracture surface of 100 and 100H 67
Figure 87. Fracture surface of 200 and 200H 67
Figure 88. Fracture surface of 200 and 200H 67
Figure 89. Fatigue crack growth (left) and fast fracture region (right) of 100 68
Figure 90. Fatigue crack growth (left) and fast fracture region (right) of 100H..... 68
Figure 91. Fatigue crack growth region of 200..... 68
Figure 92. Fatigue crack growth (left) and fast fracture region (right) of 200H..... 69
Figure 93. Fatigue crack growth (lef) and fast fracture region (right) of 300 69
Figure 94. Fatigue crack growth (left) and fast fracture (right) region of 300H..... 69

LIST OF ABBREVIATIONS

BCC	Body Centered Cubic
FCC	Face Centered Cubic
HCP	Hexagonal Closed Packed
ASTM	American Society for Testing and Materials
HV1	Vickers Hardness with Test Load of 1 kgf
SEM	Scanning Electron Microscope
EDS	Energy Dispersive Spectroscopy
CCT	Continuous Cooling Transformation
TTT	Time Temperature Transformation
C-R	Circumferential-Radial

CHAPTER 1

INTRODUCTION

For many years, the importance of more robust and corrosion-resistant high-performance materials has continued to increase significantly in room and high-temperature applications. Designers have studied materials that provide high-temperature engineering requirements. [1] For this aim, stainless steel was developed in the 1920s. [2] Soon after that, performance improvement studies were started due to the limited strength capabilities of stainless steels. Following the searches, a new type of material class is developed, named superalloys, increasing the amount of some alloys such as Cr, Al, and Mo in the structure. Superalloys are used at elevated temperatures as their mechanical and chemical degradation resistance are high at elevated temperature applications due to prominent levels of chromium in the structure. [3] Other alloys, such as ordinary steel and titanium, are not as strong as superalloys for above 540°C applications. Only refractory metals and ceramics have higher melting points than superalloys. Although ceramics possess perfect elevated temperature and corrosion resistance, their fracture toughness are not enough for structural application requirements. [1, 4]

1.1 Motivation

Fe-Ni-based superalloys have a combination of low and high-temperature strength, ductility, and corrosion resistance. Even though Fe-Ni-based superalloys can be used at lower temperatures than other types of superalloys, they are preferred in many applications due to their lower cost. Fe-Ni-based superalloys contain many alloying elements affecting mechanical properties like Fe, Ni, Cr, Al, and Mo. Different alloying elements promote different phases after heat treatment. So, all mechanical results are affected by these differences.

The primary motivation of this study is to understand the effect of phase formation after heat treatment on the characterization and mechanical properties of different Fe-Ni-based superalloys.

CHAPTER 2

LITERATURE REVIEW

2.1 General Information About Superalloys

Superalloys, known as high-temperature resistance materials, have high creep and corrosion resistance and strength because of different alloying elements in their structure such as Cr, Al, Mo, Nb, and Co. At elevated temperatures, all superalloys' creep, and corrosion resistance e higher than stainless steels. [5, 6] The variation of creep and corrosion resistance with temperature are shown for varied materials in Figure 1.

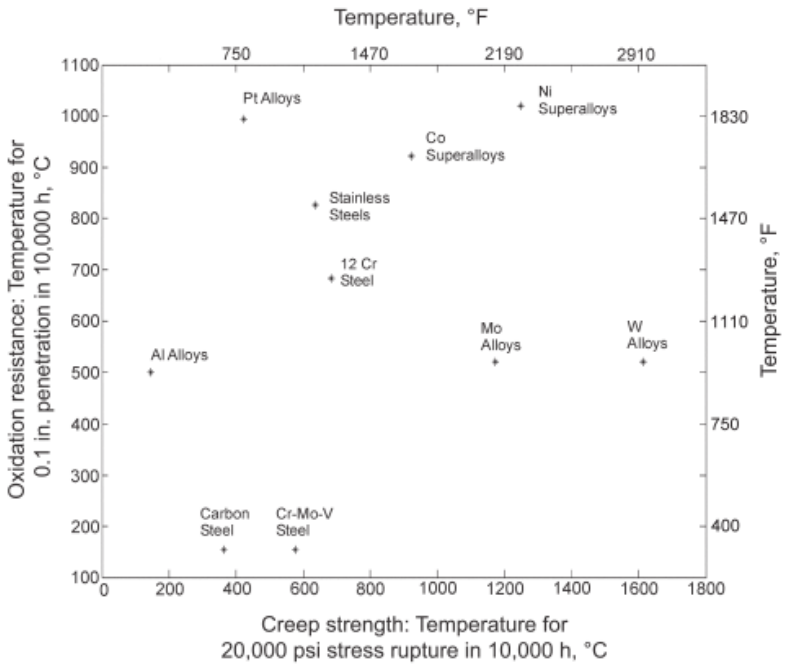

Figure 1. Creep strength and oxidation resistance of some materials with temperature [3]

Superalloys are preferred primarily on parts working at elevated temperatures. The hot section of a gas turbine engine is the primary example of the application area of superalloys. Due to their superior properties, superalloys are used in many rooms and elevated temperature applications like rocket components, nuclear reactors, furnaces used in industry, heat exchangers, petrochemical equipment, equipment used in petroleum production, automotive turbochargers, and biomedical devices. In detail, disks, bolts, shafts, cases, blades, and vanes are made up of superalloys in aircraft and industrial gas turbine components. Also, the other application areas of superalloys are hot work tools and die, casting dies, dentistry devices, trays, fixtures, conveyor belts, and nuclear power systems. [2, 7, 5, 6]

2.2 Types of Superalloys

According to the base elements, there are three types of superalloys: Fe-based (Fe-Ni-based), Ni-based, and Co-based superalloys. [4] The strength properties of these types of superalloys are directly related not only to the chemistry of the alloy but also to working processes and heat treatment. [2]

All superalloys possess a similar microstructure, a face-centered cubic (fcc) matrix with several precipitated secondary strengthening phases. [8] Only nickel has an fcc crystal structure in base metals at room temperature, but other base metals, Fe and Co, are not in the fcc structure at that temperature. The first one has body-centered cubic (bcc) and the second one possesses hexagonally close-packed (hcp) at room temperature (Figure 2). They alter their crystal structures at elevated temperatures. While the transformation temperature is 417°C for Fe, this temperature is 912°C for Co. In superalloys, fcc structure stabilization is achieved by adding nickel at low temperatures. [2, 3, 7, 5]

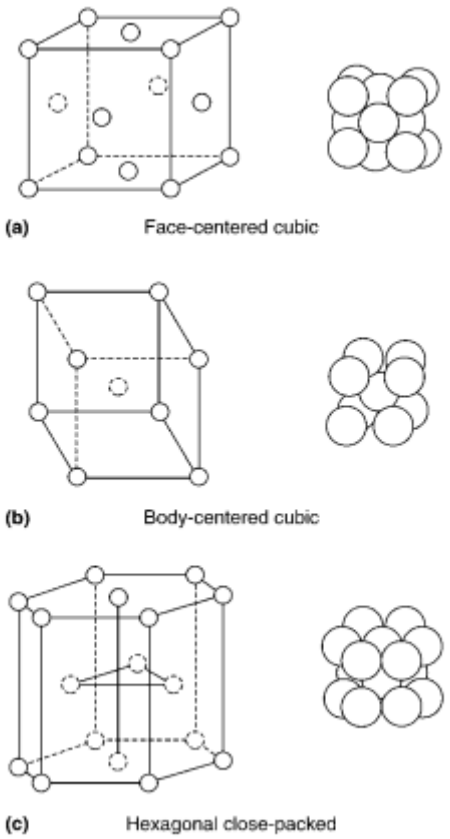

Figure 2. Crystal structures in superalloys [2]

2.2.1 Ni-Based Superalloys

Ni-based superalloys are generally preferred for parts with the highest temperature of about 1204°C to 1371°C. Nickel-base superalloys possess the highest strength at the most elevated temperatures compared to other alloys. This situation allows this type of superalloy to be used in demanding applications like turbine blades. [9] Moreover, nickel-base superalloys are generally preferred in some parts of turbine discs and forged blade, which requires high toughness. [10]

Ni-based superalloys contain 15-25% Cr, 50-70%Ni, 2.5%Co, 10-15%Mo, 2-10%Fe, and others on average. [1]

2.2.2 Co-Based Superalloys

Cobalt-base superalloys have higher melting temperatures than other types of superalloys due to the higher melting point of base metal Co. They are high-temperature and high-temperature corrosion applications. Thermal fatigue resistance and weldability of Co-based superalloys are higher than Ni-based superalloys. [10]

20-30% Cr, 35-55%Co, 10-20%Ni, 4-8%Mo, and some other elements like W, Nb, Ti, and Fe are present in Co-based superalloys. [1]

2.2.3 Fe-Ni Based Superalloys

Fe-Ni-based superalloys are one of the most useful type of superalloys because of not only their high strength, toughness, and ductility aspects but also their lower cost. [11] Iron-nickel-based superalloys may be more beneficial at moderate temperatures than cobalt- or nickel-base superalloys if the high strength is not necessary. Also, Fe-based superalloys are less expensive than other types due to iron addition in the structure. Fe-based superalloys are tough and ductile materials used in several areas, like turbine discs or forged rotors. Iron-based superalloys are one of the most useful type of superalloys since not only their high strength, toughness, and ductility aspects but also their lower cost. [10]

Fe-Ni-based superalloy contains 15-20% Cr, 25-40%Ni, 1-5%Mo, 1-3%Ti, 45-55%Fe and others. [1]

2.2.3.1 Chemical Composition of Fe-Ni-Based Superalloys

In Fe-Ni-based superalloys, Fe is the based element. Fe-Ni-based superalloys are alloys strengthened by intermetallic compound precipitation in an fcc matrix. Iron is not in fcc structure at room temperature like cobalt. Ni addition gains to the fcc matrix in the Fe-based superalloys.

Reliable mechanical properties of the Fe-based superalloys depend on their production routines, like cast and wrought, chemical composition, and strengthening mechanisms like precipitation hardening with heat treatment. [2]

Iron

Iron is used with nickel in the superalloy as a based metal due to the poor properties of iron. Nickel is added into the iron matrix Fe-Ni-based based superalloys. Iron improves workability. Instead, iron is preferred as based metal due to its lower cost than nickel or cobalt.

Nickel

Ni is used for fcc stabilizer at room temperature in the Fe-Ni-based superalloys. It provides γ' formation with titanium and, γ' is the main strengthening phase in this type of superalloy.

Chromium

Most of the entire superalloys contain chromium which affects mechanical properties and environmental resistance. Chromium is essential in secondary carbide formation ($M_{23}C_6$ and M_6C) from the primary carbides (MC and M_6C). These secondary carbides enhance the strengthening of the Fe-Ni-based superalloys.

Aluminum

Aluminum possesses similar aspects as chromium, which is a significant factor in enhancing mechanical properties and environmental resistance. However, excessive aluminum addition degrades ductility for Fe-Ni- based superalloys. So, it is present at most 0.5% in the structure. [1]

Titanium

Titanium encourages the formation of γ' precipitates, and it is, more effective than aluminum in raising the solvus temperature, and lattice parameter of the γ' phase

Titanium provides additional strengthening by increasing the antiphase-boundary energy for γ′. Titanium is also a strong MC-type carbide former.

Molybdenum

The effect of molybdenum on superalloy properties is not limited to tensile strength. Like all refractory elements, its large atomic size leads to inherently low diffusivity, which results in improved creep properties for the alloy with higher molybdenum contents.

Carbon

Carbon contributes to the properties of the solidified metal. As in steels, carbon plays a vital role in superalloys, even at low concentrations (less than one weight percent and commonly less than 0.1 weight percent). Its main effect on mechanical properties is strengthening via the formation of carbides. Carbon, at levels of 0.02 to 0.2 weight percent, combines with reactive and refractory elements such as titanium, and tantalum to form primary MC carbides. During heat treatment and service, these MC carbides into secondary carbides such as $M_{23}C_6$ and M_6C, which tend to populate grain boundaries and improve superalloys' mechanical properties.

Table 1. Effects of elements in Fe-Ni-based superalloys [2]

Elements	*Properties in Superalloys*
Ni	It helps in the formation of γ′ phase
	Provide good thermal stability and fabricability
Cr	Solid solution hardening via precipitation of $M_{23}C_6$
	Enormous amounts of Cr decrease the precipitated fraction of γ′ phase
Al	Helps in the precipitation of γ′ phase Ni_3(Ti, Al)
	Suppress precipitation of η phase (Ni_3Ti)
Ti	Helps in the precipitation of γ′ phase Ni_3(Ti, Al)
C	Solid solution hardening by precipitation of $M_{23}C_6$, M_6C, and MC
Mo	Solid solution hardening by precipitation of M_6C

2.2.3.2 Phases and Their Effects on Fe- Ni-Based Superalloys

The austenitic fcc structure is the main matrix of the superalloys due to Ni content in the structure matrix phase, γ, and a variety of secondary phases. [5, 4] Secondary phases are effective on properties of Fe-Ni-based superalloys, which are MC, $M_{23}C_6$, M_6C, and M_7C_3. Gamma prime (γ′) fcc ordered Ni_3(Al, Ti), gamma double prime (γ″) bct ordered Ni_3Nb, eta (η) hexagonal ordered Ni_3Ti, and the delta (δ) orthorhombic Ni_3Nb intermetallic compounds are existed in Fe-Ni based superalloys depend on the alloying element types, amount and sizes and also heat treatment. [2, 6, 12]. Precipitated phases, after precipitation hardening heat treatment, generally improve the strength of superalloys. In most cases, γ′ and γ″, phases are formed in iron-nickel-base superalloys with precipitation hardening. [11] Carbides may provide strengthening by strengthening grain boundaries against plastic deformations. Three types of superalloys consist of these carbides.

Table 2. Phases in Fe-Ni-based superalloys [13]

Phases	*Crystal Structure*	*Information*
γ′ **Ni_3Al** **Ni_3(Al, Ti)**	fcc	The principal strengthening phase, is spherical, in nickel-iron-base superalloys, and its size varies with exposure and heat treatment time and temperature.
MC **TiC**	cubic	Composition is variable; it appears as globular, irregularly shaped particles.
$M_{23}C_6$ **$Cr_{23}C_6$**	fcc	It can precipitate as films, globules, platelets, lamellae, and cells; it usually forms at grain boundaries.

Table 2(Cont'd)

M_6C **Fe_3Mo_3C,**	fcc	-
M_3B_2 **Ta_3B_2** **V_3B_2** **Nb_3B_2**	tetragonal	Borides appear like carbides but are not attacked by preferential carbide etchants.

2.3 Heat Treatment of Fe-Ni-Based Superalloys

Heat treatment is applied on almost all materials for suitable purposes, as shown below:

- Stress reduction
- Alloying element movement and redistribution
- Recrystallization of grains
- Phase dissolution
- New phases production
- Strength and toughness improvement
- Improvement of machining by softening heat treatment

Several types of heat treatment procedures are also used for superalloys. Heat treatment is an essential method for modifying the size and amount of the precipitates in the structure. [3]

2.3.1 Heat Treatment Types for Fe-Ni-Based Superalloy

Depending on various requirements, different heat treatments can be applied to Fe-Ni-based superalloys. [14] Homogenization heat treatment is performed to reduce

compositional gradients, and a more uniform structure is obtained at the end of this heat treatment. Another heat treatment is stress relief heat treatment for Fe-Ni-based superalloys. The main goal of stress-relieving superalloys is the elimination of stress in the structure after welding, machining, thermal shock, etc. In this heat treatment, time and temperature cycles depend on not only characteristics but also the development of type and magnitude of residual stress in the structure during working processes. Annealing heat treatment, the other heat treatment procedures, is used in all material types. Annealing is used to increase ductility, reduce hardness, and homogenize a cast ingot. This makes forming and machining easier. In addition, it provides the elimination of stress after welding. Heat treatment is also preferred for the strengthening of superalloys. Precipitation hardening to apply on age-hardenable alloys for strengthening. There are two main stages in precipitation hardening. The first stage is solution heat treatment and fast cooling with a quenching agent such as water. In solution heat treatment, precipitates dissolve partially or wholly in the structure. The second stage is aging. In aging, the dissolved elements precipitate in a type and morphology. [12]

2.3.2 Strengthening for Fe-Ni-Based Superalloy

Fe-Ni-based superalloys are strengthened by precipitation hardening. It is achieved by precipitating of γ', γ'', η, and carbides in the structure and at the grain boundary. The other strengthening mechanism is solid solution hardening. [15, 16, 3] It is obtained with dissolution of elements in the matrix. In addition, Fe-Ni-based superalloys are also strengthened with grain refinement. Grain refinement is obtained if crystal structure changes during heat treatment. If not, thermomechanical deformation or hard working is required for grain refinement. [17, 18, 19]

2.3.3 Effect of Solution Heat Treatment and Aging on Microstructure and Mechanical Properties of Fe-Ni-Based Superalloys

Precipitation hardening is one of the strengthening mechanisms for superalloys. After heat treatment, different phases and carbides are expected to precipitate in the matrix or grain boundary. However, their shape, size, and types change with changing heat treatment parameters such as temperature and time.

2.3.3.1 Microstructure

After solution heat treatment and aging, γ′ and γ″, phases are formed in an iron-nickel-base superalloy microstructure. γ′, the principal strengthening phase, is spherical, in nickel-iron-base superalloys and its size varies with exposure and heat treatment time and temperature. Size of γ′ increases with increasing aging time and temperature. In fact, γ′ dissolves to η phase with prolonged aging.

In addition, carbides ($Cr_{23}C_6$) may provide strengthening by strengthening grain boundaries against plastic deformations. It can precipitate as films, globules, platelets, lamellae, and cells; it usually forms at grain boundaries. A general schematic representation of the microstructure is shown below (Figure 3). [3]

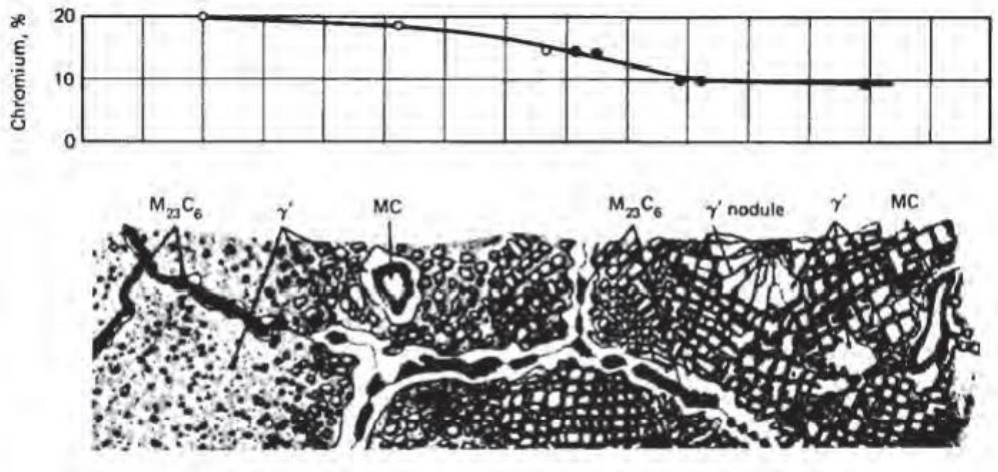

Figure 3. Schematic representation of the microstructure of Fe-Ni-based superalloys

2.3.3.2 Hardness

Hardness is changed with changing heat treatment temperature and time parameters. The increasing hardness of Fe-Ni-based superalloys is expected for two main reasons. The first one is carbide formation in the matrix or grain boundary. Presence of carbide precipitates blocks dislocation within the structure and hardness increase. The second reason is grain size refinement. After heat treatment, grain size is reduced to critical heat treatment temperature and time. The finer grain causes more build-up of dislocation at the grain edge and hardness increases. Jacuinde et al have a similar observation from their study [20].

However, an increase in solution treatment temperature results the dissolution of chromium carbide, coarser grain, and lower hardness. This finding is like being observed by Ridhwan and Wang. Grain coarsening occurred due to increasing temperature and time causing lower hardness in Fe-Ni-Cr steel. [21, 22]

2.3.3.3 Tensile Test

The tensile strength of Fe-Ni-based superalloys has a similar aspect to hardness. Dislocation motion is blocked with increasing carbide forming and grain size decreasing. More energy is required for it. If the solution heat treatment and aging temperature and time increase, carbides grow and dissolve. Also grain growth can be seen. So, strength is reduced. Zhao et al. investigate similar effect in their study. They show that the strength of Fe-Ni-based superalloys increases with increasing carbide particle amount and size until the critical size [6].

2.3.3.4 Fatigue crack growth

Designers take all measurements into account to minimize fatigue failures, materials are not free of defects. There are always cracks and nucleation sites in structural component of materials. [23] In addition, most of the engineering components

exposed to cyclic stresses and strains which cause fatigue failure. So, fatigue failure is an essential case for most of materials. In fatigue failure, repeated and cyclic stress below yield strength of the material is applied. It causes crack formation, propagation, and failure. [24] As a result of that, the life of designed component has a correlation with rate of fatigue propagation.

There are experimental techniques such as fatigue crack growth test, to detect crack size under cyclic loading. In this test, crack size is measured for each number of cycles. After that, all data are collected, crack size graph is drawn versus number of cycle (Figure 4). Fatigue crack growth rate can be evaluated from slope of crack size (a) – number of cycle (N) graph.

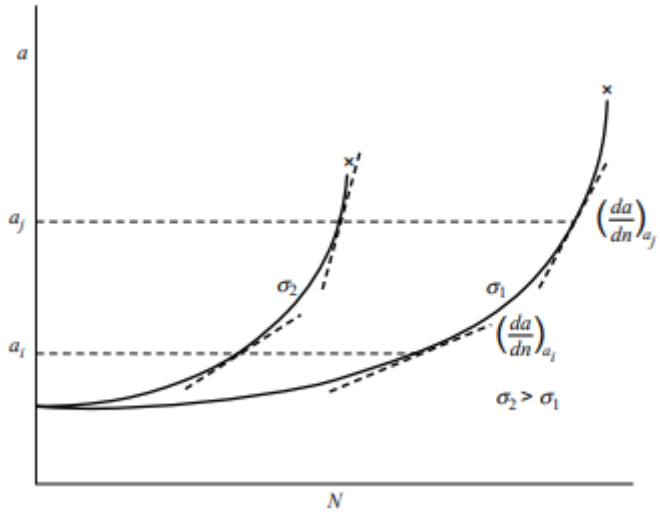

Figure 4. a-N curve [25]

Experiments done on fatigue crack growth rate for all metallic materials have illustrated that the da/dN versus ΔK curves have three distinguishable regions.

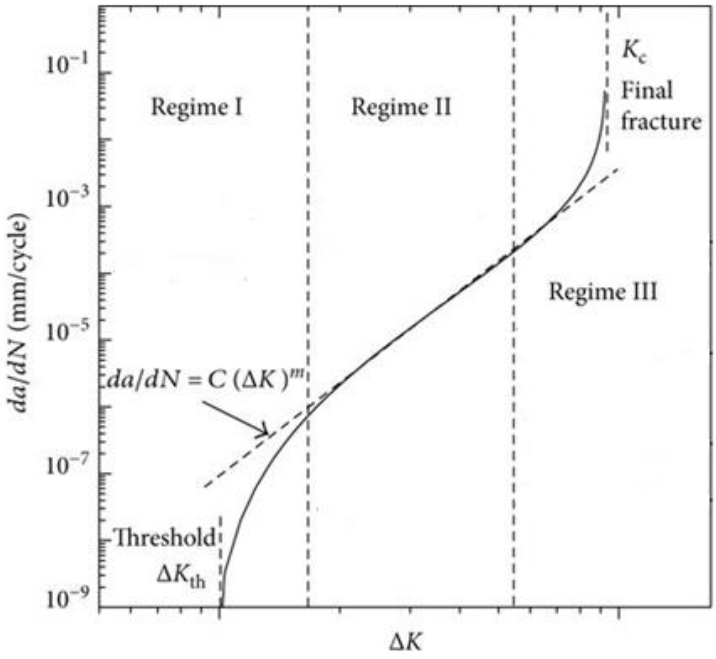

Figure 5. da/dN versus ΔK curves for fatigue crack growth [26]

In da/dN versus ΔK curves possess three distinguishable regions. In the first region, crack growth rate is low and crack growth rate increase with cyclinc loading. The fatigue crack propagation threshold can be seen in the first region of the curve. Below the treshold value, there is no crack propagation. The second region crack propation increase linearly. In this region, logda/dN and logΔK have linear relation ship and this relation is explained with Paris-Erdoğan equation as shown below. So, this region is also known as Paris-Erdoğan region. The last region is fast fracture region and crack propagation is reached the highest value. In this region catastrophic failure occurs and ΔK value is close to the K_C or K_{IC} value. [27]

$$\frac{da}{dN} = C\Delta K^m$$

CHAPTER 3

EXPERIMENTAL PROCEDURE

3.1 Materials Used in Experiments

In this study, three different Fe-Ni-based superalloys are produced according to the GOST standards. There is no AISI equivalent of these three alloys. All alloys have different alloying elements like Cr, Mo, Al, etc. All samples are identified with a numerical number as shown in Table 3. The diameter of each sample is also different from each other. The diameter of the first sample, 1xx, is 30mm. In addition, 2xx has 40mm diameter. The last sample, 3xx, has 45mm diameter.

Table 3. Numerical name of all samples

Samples	*General Name*	*Diameter*
1	1xx	D1
2	2xx	D2
3	3xx	D3

First sample designation is 100 for as received condition. 200 is used for Sample 2 and Sample 3 named as 300 for as received condition. After heat treatment, all samples are taken H letter.

Sample 100 is produced by forging to 40 mm. After forging, it is hot rolled to 30 mm. Other samples, Sample 200 and Sample 300 are only forged to their final dimensions.

Moreover, all samples are machined to theis test shapes before heat treatment in order to eliminate dimensional differences between the samples.

3.2 Heat Treatment

In this study, solution heat treatment and aging are preferred for three different Fe-Ni-based superalloys to observe the reaction of the alloying element against heat treatment. The same heat treatment parameters are applied since the samples have different alloying elements.

In solution heat treatment, all samples are put into the furnace at 980 °C for 1 hour as shown in Figure 6. After solution heat treatment, water quenching is applied to all samples. The solution heat treatment furnace is Lenton Thermal Designs (Figure 7).

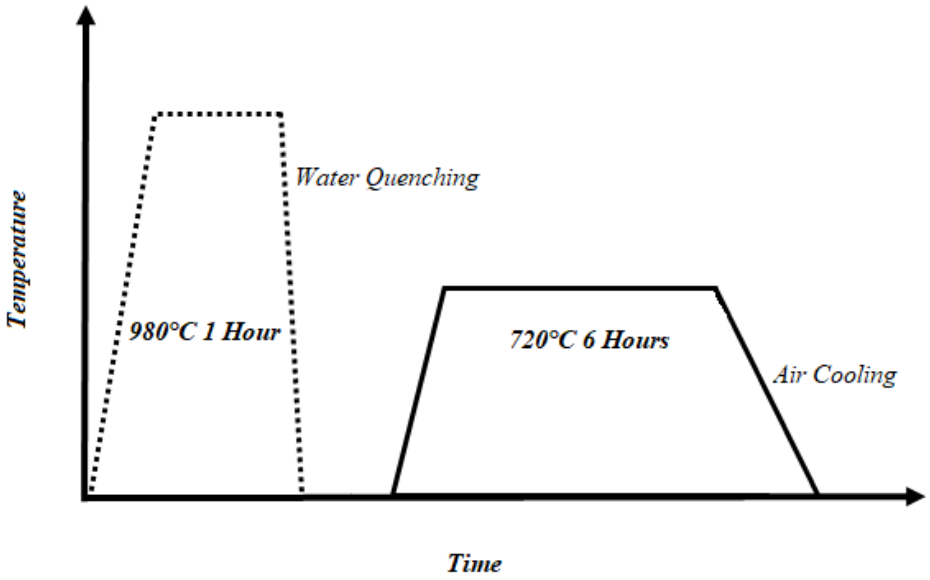

Figure 6. Heat treatment steps of Fe-Ni-based superalloys

Figure 7. Solution heat treatment furnace

After solution heat treatment, pieces are put into the furnace at 780°C for 6 hours for aging. Finally, air cooling is performed. Protherm electrical furnace (Figure 8) is used for the aging process.

Figure 8. Aging heat treatment furnace

Figure 9. All samples in the furnace for solution heat treatment and aging

3.3 Characterization Tests

3.3.1 Hardness Test

Microhardness test is performed for material characterization of received and heat-treated samples concerning ASTM E384. All measurements are taken with Shimadzu Micro Hardness Tester. Hardness measurement is taken (Figure 10) with HV1 at points in 200μm, 700μm, 1200μm, 1700μm, 3500μm, 5500μm, respectively.

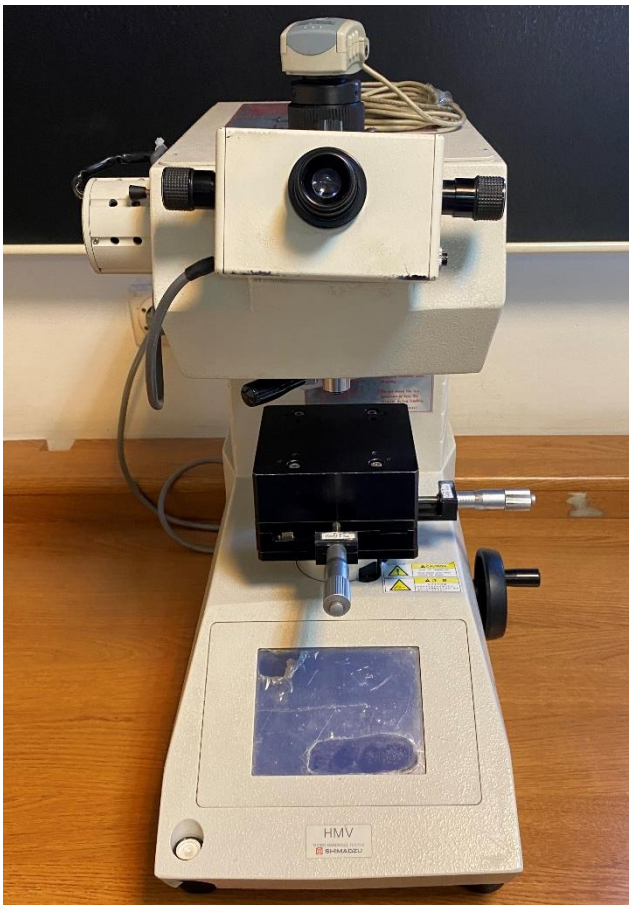

Figure 10. Micro vickers hardness tester

3.3.2 Spectral Analysis

Spectroscopic analysis is performed in Spectromaxx LMX07 Arc/Spark Optical Emission Spectroscopy Analyzer. Spectroscopic analysis is made using Ni-01-F method 42 and calibrated in this method (Figure 11). These measurements were done to each as received samples.

Figure 11. Spectroscopy analyzer

3.3.3 Microstructural Analysis

Metallography is carried out for microstructure of three different Fe-Ni based superalloys in as received and as heat treated condition. In metallograpy, cutting, taking in bakelite, grinding, polishing and etching are carried out respectively. For cutting operation Metkon Metacut 251 Abrasive Cutter is used (Figure 12).

Figure 12. Abrasive cutter

After cutting, all samples are taken in bakelite with Metkon Ecopress100 (Figure 13).

Figure 13. Bakelite machine

Later, sample preparation is started with grinding. It is worked on Metkon Gripov2V Grinder Polisher (Figure 14). Presi Mecapol P230 is used for polishing (Figure 15).

Figure 14. Grinder

Figure 15. Polisher

In etching process, Waterless Kalling's solution is prepared. After sample preperation, microstructure is characterized by Nikon Eclipse E200 Optic microscope (Figure 16) and Clemex software.

Figure 16. Optical microscope

3.3.4 Tensile Test

Tensile test specimens are prepared acording to the ASTM E8. Round specimens are prepared for the test and two tensile tests are conducted for each sample shown in Figure 17. During the test, the crosshead speed is 1 mm/min.

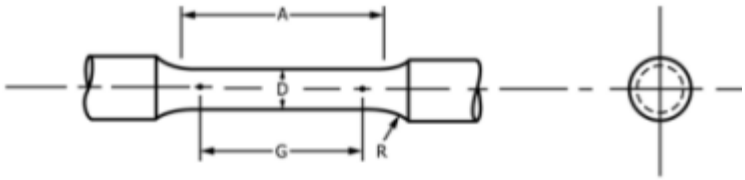

Dimensions, mm [in.]	
G—Gauge length	30.0 ± 0.1 [1.250 ± 0.005]
D—Diameter (Note 1)	6.0 ± 0.1 [0.250 ± 0.005]
R—Radius of fillet, min	6 [0.188]
A—Length of reduced parallel section, min (Note 2)	36 [1.4]

Figure 17. Tensile test specimen dimensions [28]

Figure 18. Tensile test machine

3.4 Fatigue Crack Growth Rate Test

Fatigue crack growth test is perfomed according to the ASTM E647. All test samples are prepared according to ASTM E399, shown in Figure 19.

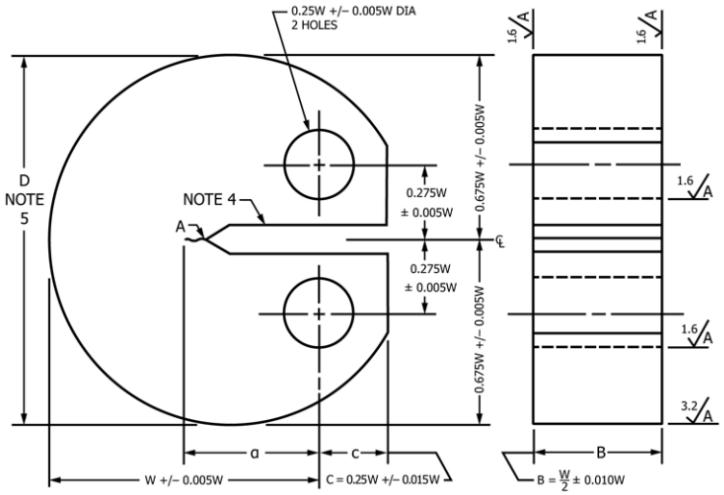

Figure 19. Fatigue crack growth test specimen dimensions [29]

According to the standard, all samples prepared along C-R direction (Figure 20).

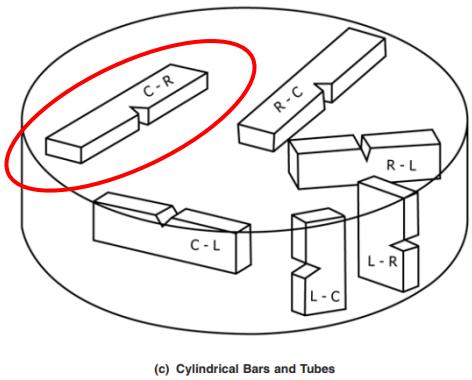

Figure 20. Fatigue crack growth sample production dimensions [29]

Crack growth test is performed in MTS Universal Fatigue Machine (Figure 21) During the test, datas are collected from lines drawn on the sample surface at 1 mm intervals as shown in Figure 22. In addition, more datas are taken from photos taken every 30 seconds (Figure 23).

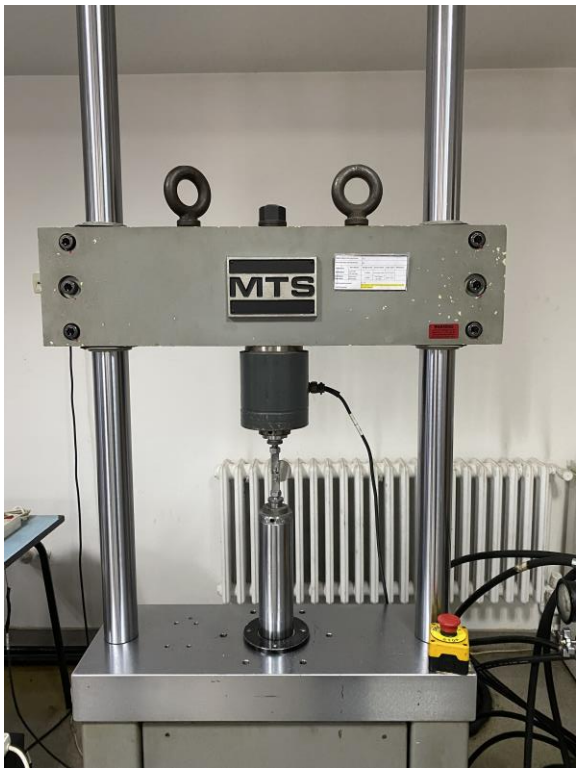

Figure 21. Universal fatigue crack growth machine

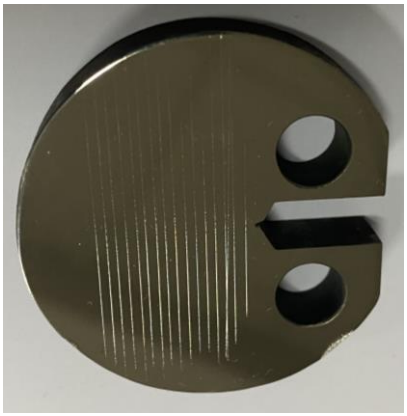

Figure 22. Fatigue crack growth sample and drawn lines

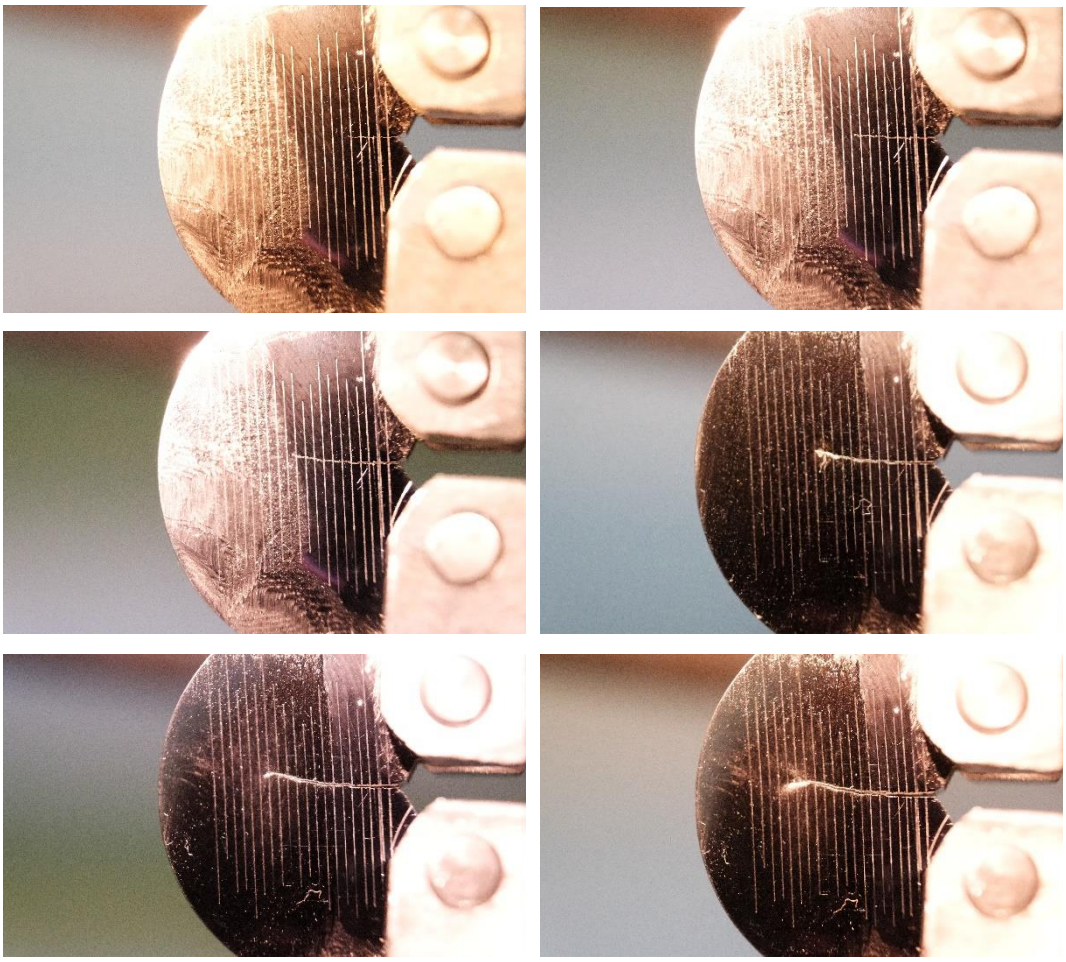

Figure 23. Fatigue crack growth samples from test

In the fatigue crack growth test, constant load and frequency are used for each test group. R values are taken as 0.1 for all samples. The loading is applied in sinusoidal form as shown in Figure 24. Values for the test also are listed in Table 4.

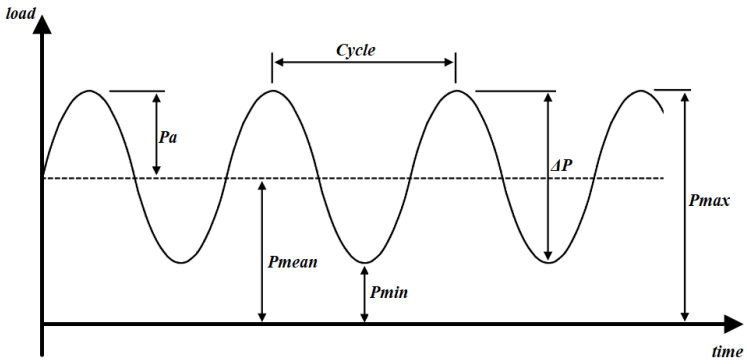

Figure 24. Loading during fatigue crack growth test

$$R = \frac{Pmin}{Pmax}$$

$$Pmean = \frac{Pmin + Pmax}{2}$$

$$Pamplitute = Pmax - Pmean$$

$$Pamplitute = Pmean - Pmin$$

Table 4. Test load and frequency parameters

Samples	P_{mean} (N)	$P_{amplitude}$ (N)	frequency (Hz)
D1 Sample 106 & Sample 406	2750	2250	14.0
D2 Sample 206 & Sample 506	4400	3600	14.0
D3 Sample 306 & Sample 606	6325	5175	10.0

Some photographs are shown in Figure 25 during the test.

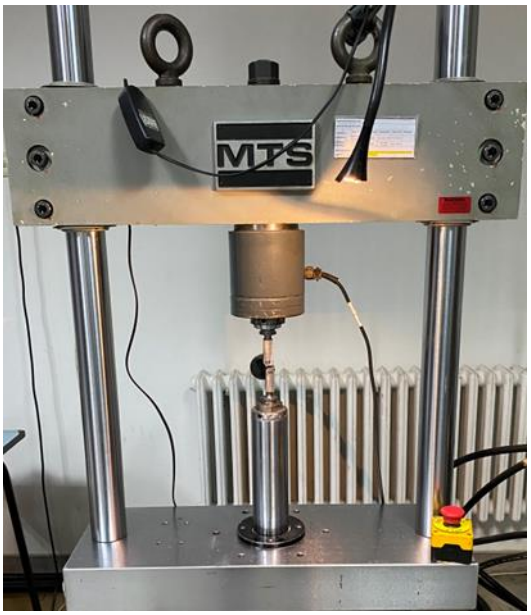

Figure 25. Crack growth test setup

CHAPTER 4

RESULTS & DISCUSSION

In this chapter, all the results of the study carried out in the thesis study are explained below in titles. After the heat treatment is performed, the characterization results and their discussions are included. Later, mechanical properties are evaluated.

4.1 Material Characterization Results

4.1.1 Chemical Composition Analysis Results

The chemical compositions of 3 different Fe-Ni-Based superalloys are shown in Table 5. This analysis is applied only to as received samples.

Table 5. Chemical compositions of three different samples

	Ni	*Fe*	*Cr*	*Ti*	*Al*	*Si*	*C*	*Mo*	*W*	*Other*
Sample 100	35,21	46,62	11,82	2,60	0,95	0,73	0,03	0,13	0,24	Balance
Sample 200	43,18	47,95	4,95	1,82	0,45	0,55	0,03	0,05	0,15	Balance
Sample 300	46,20	45,02	4,80	2,05	0,56	0,65	0,03	0,04	0,10	Balance

Chemical composition of samples are different from each other. Their Fe and C content are similar but other elements change in samples. While Sample 200 and Sample 300 have almost similar Ni content, Sample 100 has lower Ni content than other samples. On the contrary, Sample 100 has much higher Cr than the others. All test results give detailed information about chemical composition effects against heat treatment.

Aluminum is also γ' (Ni_3Al) former with Ni and it enhances mechanical properties and environmental resistance. However, excess amount of auminum in the structure

reduces ductility of Fe-Ni-based superalloys. Its content is generally less than 0.5% in the structure. Samples 200 and 300 have similar aluminum content around 0.5%. On the contrary, Sample 100 possesses much higher aluminum (0.95%). Other elements such as W, Si, and C are present in the similar amount.

4.1.2 Hardness Test Results

Initially, hardness results are compared between as received and as heat treated condition for each sample respectively (Figure 26, 27, and 28).

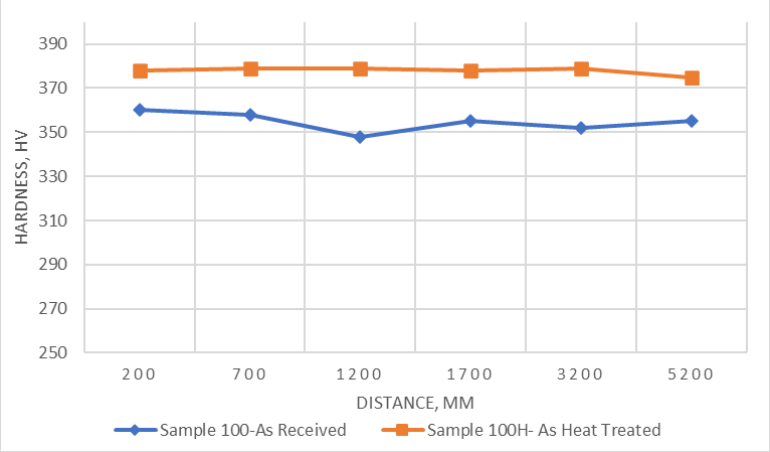

Figure 26. Hardness results of 100 (as received) and 100H (as heat treated)

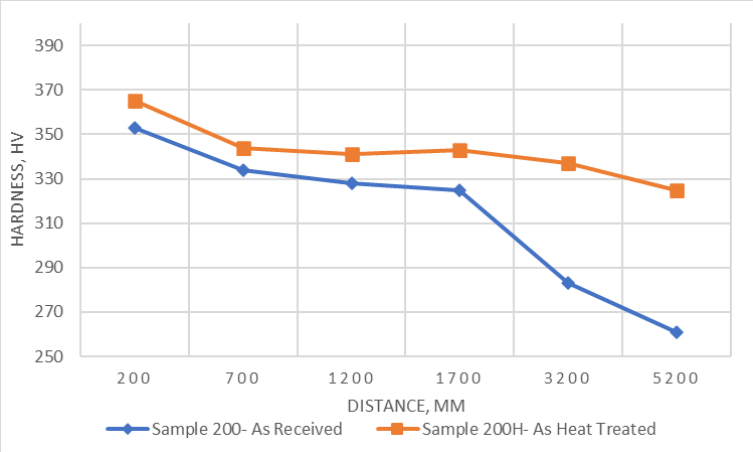

Figure 27. Hardness results of 200 (as received) and 200H (as heat treated)

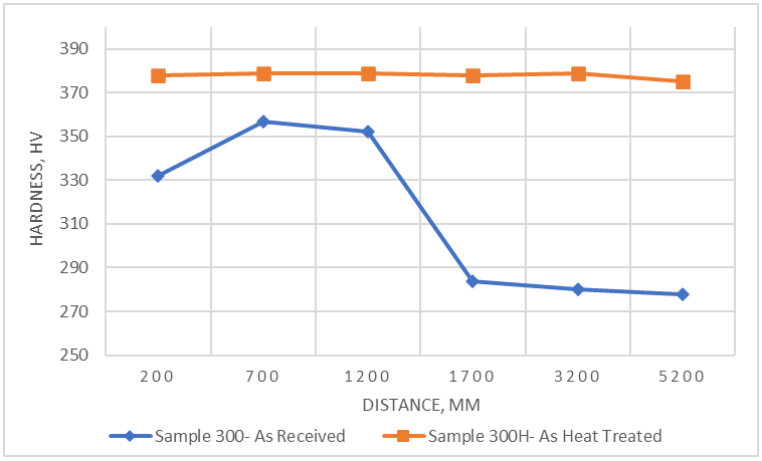

Figure 28. Hardness results of 300 (as received) and 300H (as heat treated)

According to the results, hardness values of all samples are increased with solution heat treatment and aging processes. First, 100 (as received) and 100H (as heat treated) is compared. Sample 100 has 350-360 HV1 hardness while heat treated sample, sample 100H, has 370-380 HV1 hardness. Equivalent results are collected from other samples. Hardness is affected by γ′ formation in both matrix and grain boundary with heat treatment. γ′ is the main strengthening mechanism of Fe-Ni-based superalloys and hardness is increased by heat treatment. After each sample compasion, effect of heat treatment and chemical composition are shown. Firstly, as received condition graph is represented in Figure 29. After that heat-treated condition graph is shown in Figure 30.

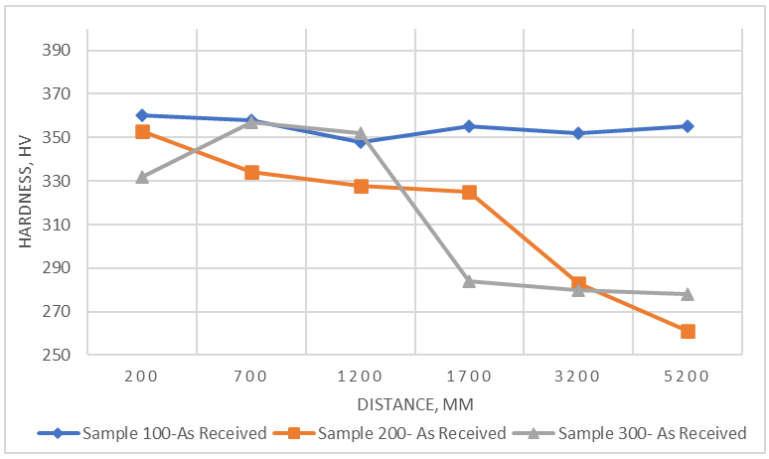

Figure 29. Hardness results of 100, 200, and 300 (as received)

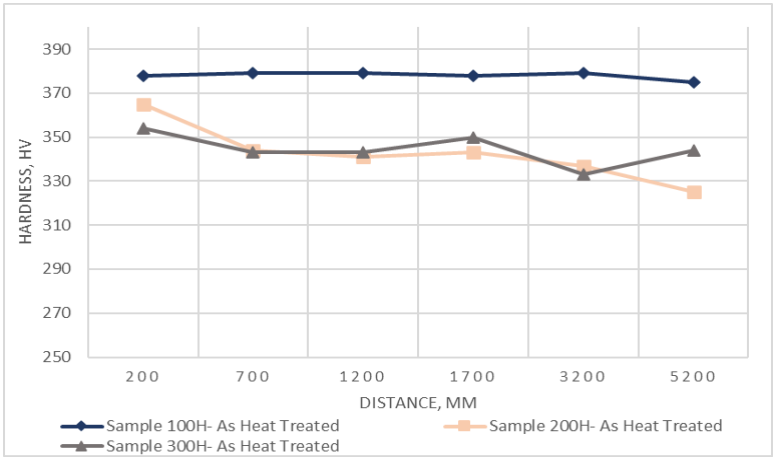

Figure 30. Hardness results of 100H, 200H, and 300H (as heat treated)

For all samples, hardness values are collected from 200, 700, 1200, 1700, 3200- and 5200-micron depth. In Sample 100, hardness values are not changed from surface to core. On the contrary, hardness values of Sample 200 and 300 are decreased dramaticly from surface to core. For instance, the surface hardness of Sample 200 is around 350 HV1 but core hardness of it is around 260 HV1. Same result is observed in Sample 300. Hardness of the sample change 360 HV1 to 280 HV1. This can be explained that sample 200 have higher chromium and molibdenum content than the others. They provide structure stabilizing. Moreover, hardness values are taken from tensile test specimens. Local hardening can be obtained from machining proceses. This nonhomogeneus properties are eliminated with heat treatment. This idea is supported with heat treated results. All hardness values are taken from similar hardness range.

4.1.3 Tensile Test Results

At the beginning, tensile test results are compared between as received and as heat treated condition for each sample respectively in Figure 31, 32 and 33.

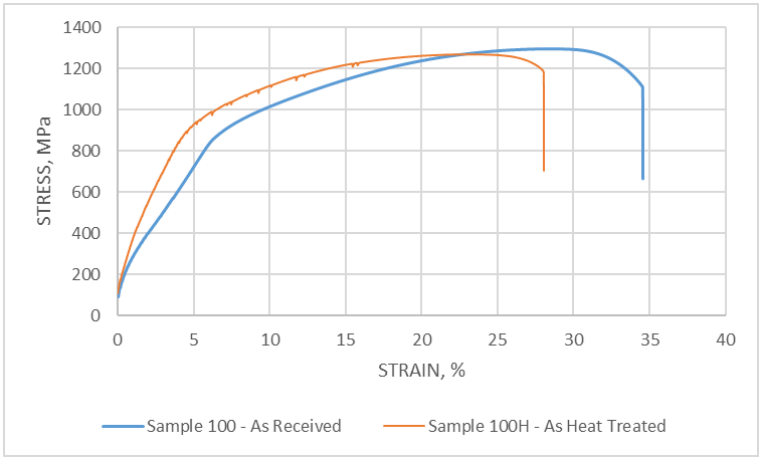

Figure 31. Tensile test results of 100 (as received) and 100H (as heat treated)

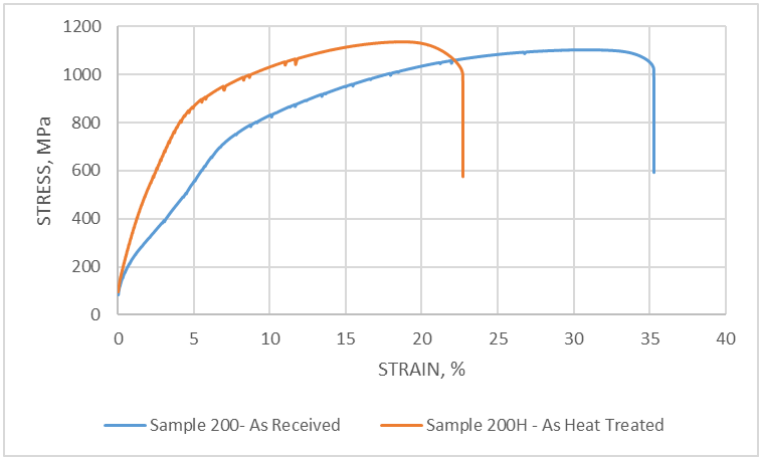

Figure 32. Tensile test results of 200 (as received) and 200H (as heat treated)

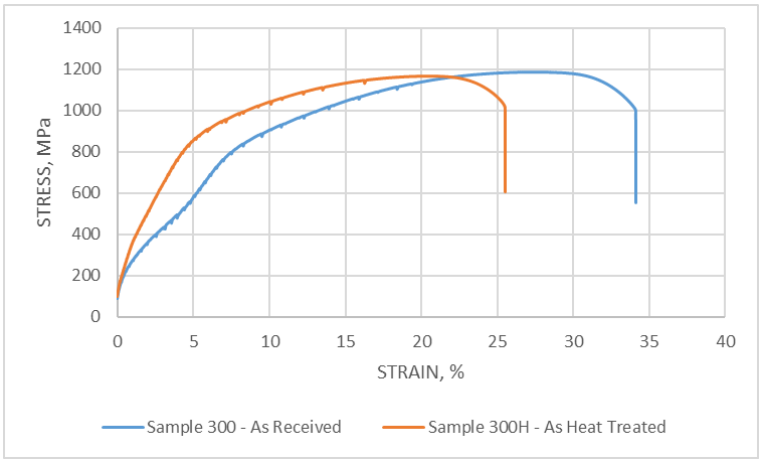

Figure 33. Tensile test results of 300 (as received) and 300H (as heat treated)

According to the results, % elongation values decrease with solution heat treatment and aging in all samples. For example, % elongation value at the rupture point is 34,5% for as received Sample 100. This value drops to around 28% with heat treatment. Same results are obtained from other samples. Stain value of Sample 200 and 300, as received samples, are approximately 35%. But this value is decreased to 23% and 25,5%, respectively. After solution heat treatment and aging, strengthening mechanism can be worked with precipitation hardening. γ' (Ni_3Al) formation are blocked dislocation motion and elongation (ductility) decreased with heat treatment.

Table 6. Mechanical properties of test samples

Sample	**Yield Strength $\sigma_y^{0.2}$ (MPa)**	**Tensile Strength σ_{UTS} (MPa)**	**% Elongation A (%)**
Sample 100	900	1280	35
Sample 100H	930	1250	28
Sample 200	780	1100	35
Sample 200H	860	1170	23
Sample 300	820	1200	34
Sample 300H	820	1180	25

It is expected that yield strength and tensile strength increase while % elongation values decrease with heat treatment. The results are shownt that yield strength of all samples increase (Table 6). However, the difference is too small to compare for sample 100. Yield strength of Sample 200 increase more than first (Sample 100) and last sample (Sample 300). In Sample 300, yield strength is not increased with heat treatment. Moreover, tensile strength decreases with this heat treatment parameter.

According to the tensile test results (Table 6), mechanical properties are slightly improved in Sample 200 because of too short aging time to precipitate of carbides. Prolonged aging time may enhance mechanical properties. On the other hand, tensile behaviour of Sample 100 and Sample 300 are not enhanced.

After each sample compasion, effect of heat treatment on chemical composition are shown. Firstly, as received condition graph is represented (Figure 34).

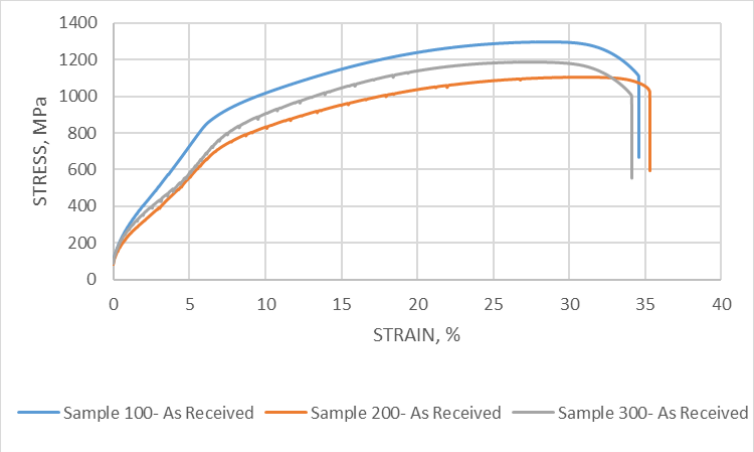

Figure 34. Tensile test results of 100, 200, and 300 (as received)

Later, tensile test results are presented for heat treated samples (Figure 35).

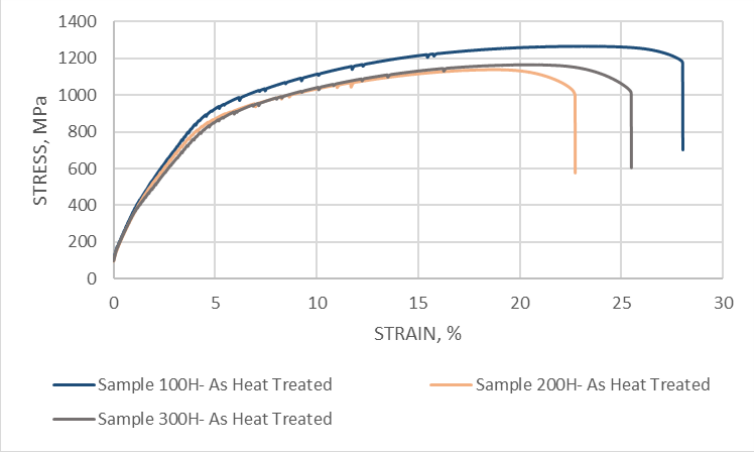

Figure 35. Tensile test results of 100H, 200H, and 300H (as heat treated)

In as received condition, Sample 100 has higher yield strength and tensile strength to compare with Sample 200 and Sample 300. Sample has higher chromium, molibdenum, titanium and molibdenum. More alloying elements can provide higher mechanical properties. Lower grain size can be results with higher mechanical properties due to blocking of dislocation motion. More energy is required for dislocation motion for low grain size samples. Grain size can be explained higher

mechanical performance of Sample 100 than others. After heat treatment, the more decreasing is observed ductility values of sample 200. However, yield and tensile strength become higher in Sample 200 than in Sample 300. On the other hand, Sample 100 possesses highest mechanical properties after heat treatment.

4.1.4 Optical Microscope Results

In optic microscope analysis, as received and heat treated are compared for each sample (Figure 36-53).

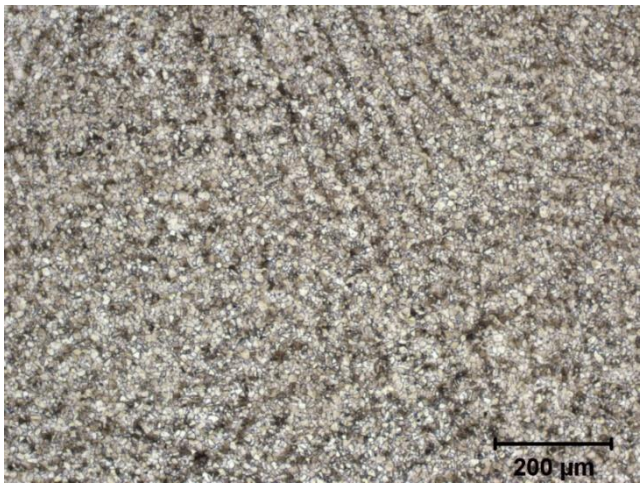

Figure 36. 100 (as received) at 100x magnification

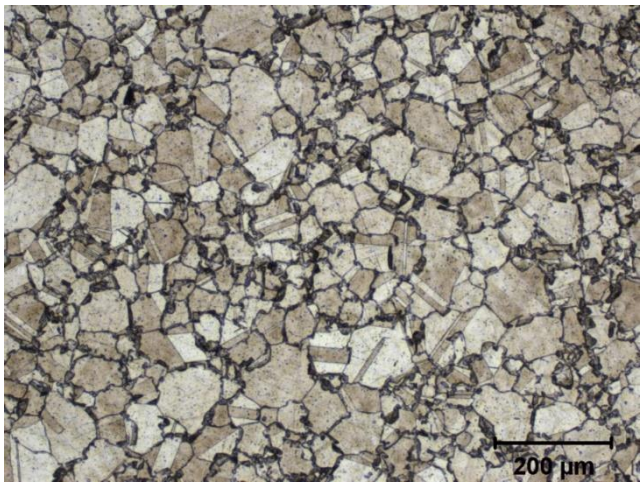

Figure 37. 100H (as heat treated) at 100x magnification

To detail, optical micrograph is taken at different magnification for same samples.

Figure 38. 100 (as received) at 200x magnification

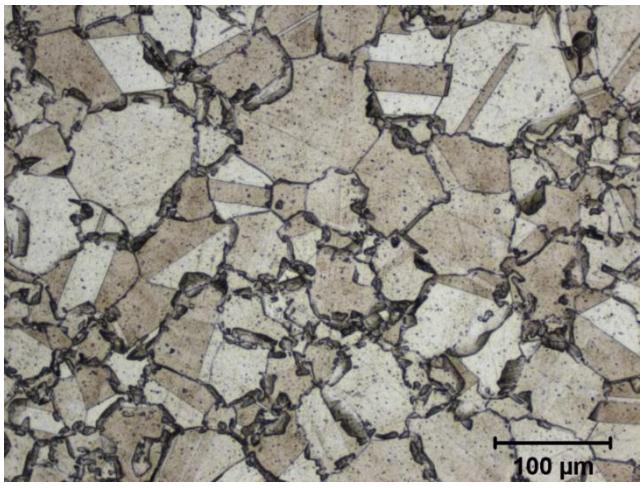

Figure 39. 100H (as heat treated) at 200x magnification

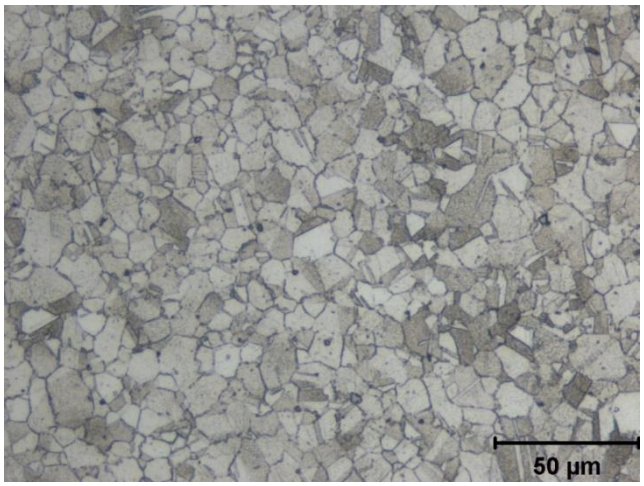

Figure 40. 100 (as received) at 500x magnification

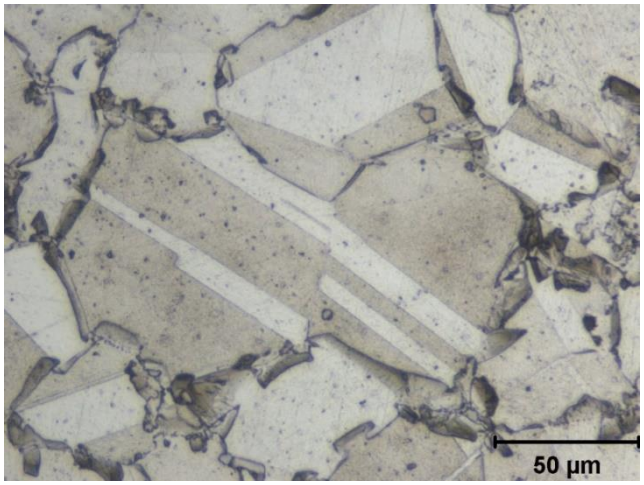

Figure 41. 100H (as heat treated) at 500x magnification

Same procedure is applied for the second sample (Sample 200 and Sample 200H) at 100x, 200x and 500x magnification.

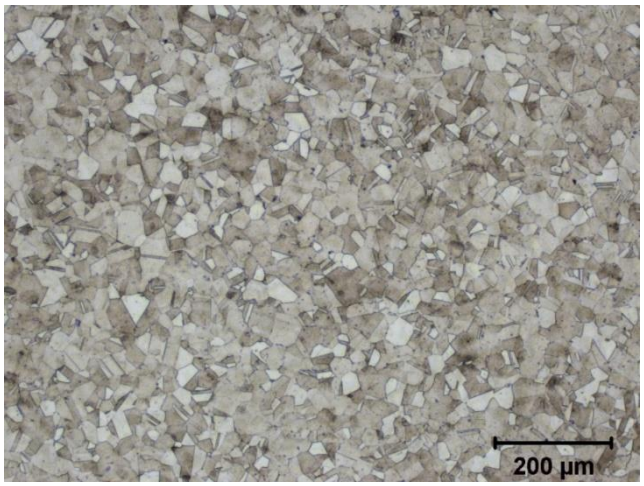

Figure 42. 200 (as received) at 100x magnification

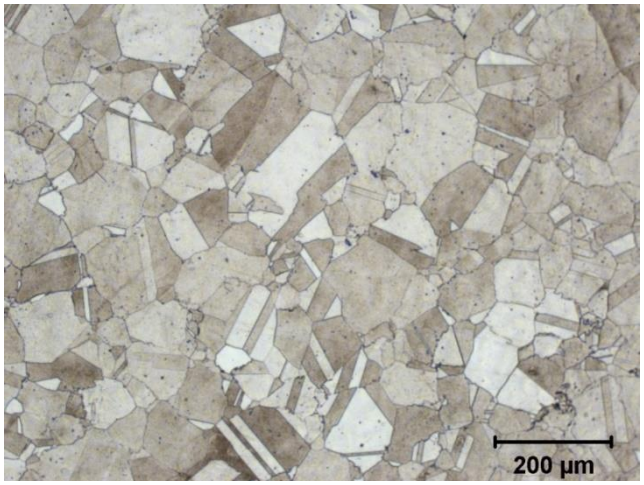

Figure 43. 200H (as heat treated) at 100x magnification

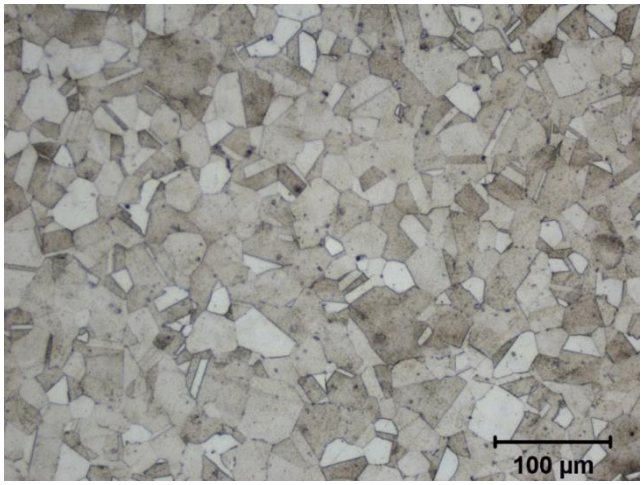

Figure 44. 200 (as received) at 200x magnification

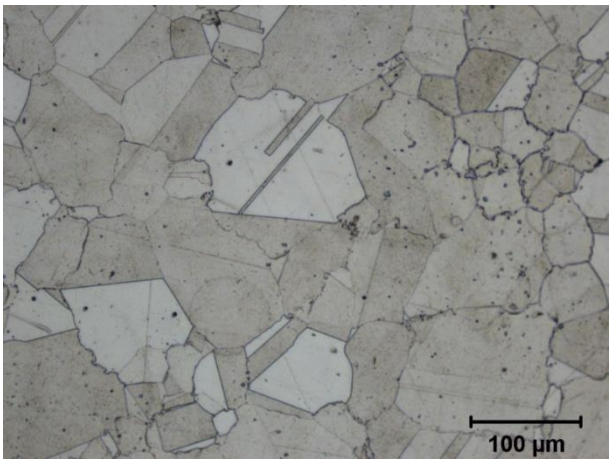

Figure 45. 200H (as heat treated) at 200x magnification

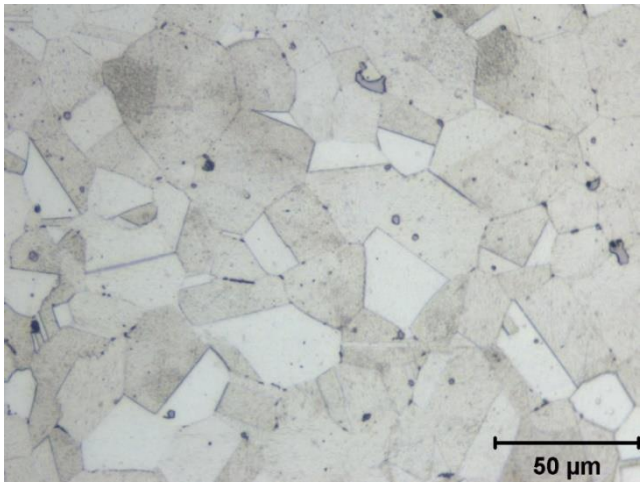

Figure 46. 200 (as received) at 500x magnification

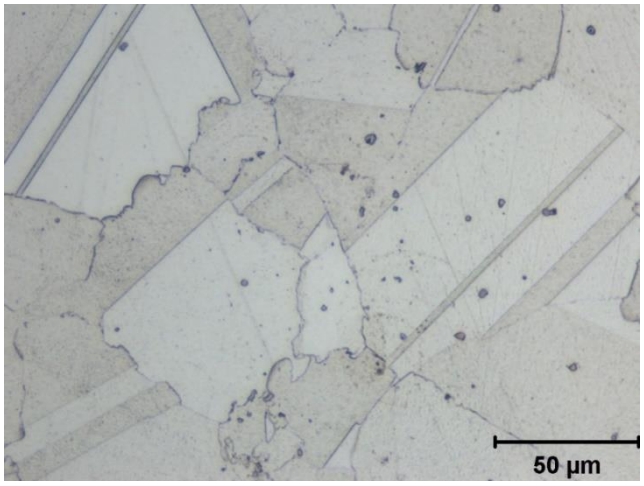

Figure 47. 200H (as heat treated) at 500x magnification

Finally, microstructure is collected for the third sample (Sample 300 and Sample 300H). at 100x, 200x and 500x magnificaiton.

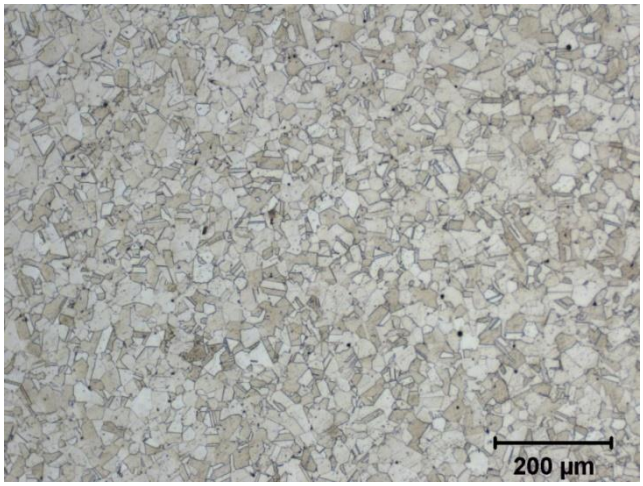

Figure 48. 300 (as received) at 100x magnification

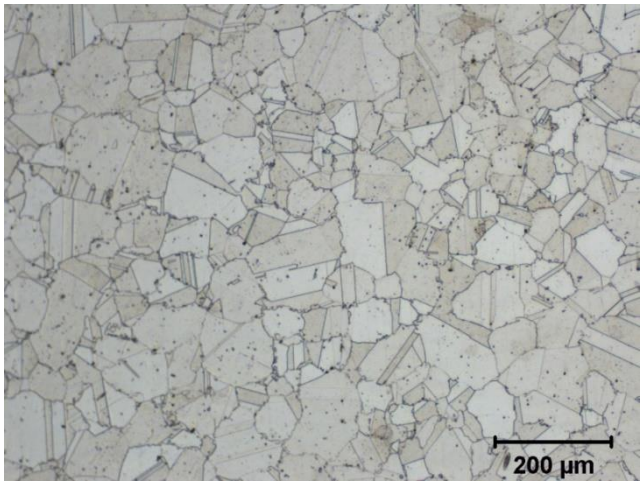

Figure 49. 300H (as heat treated) at 100x magnification

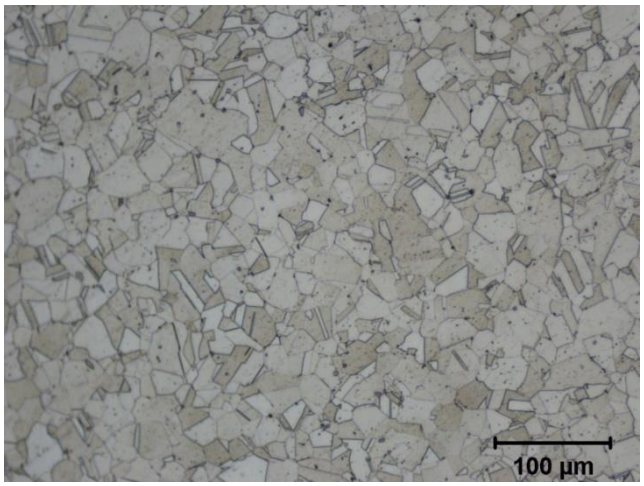

Figure 50. 300 (as received) at 200x magnification

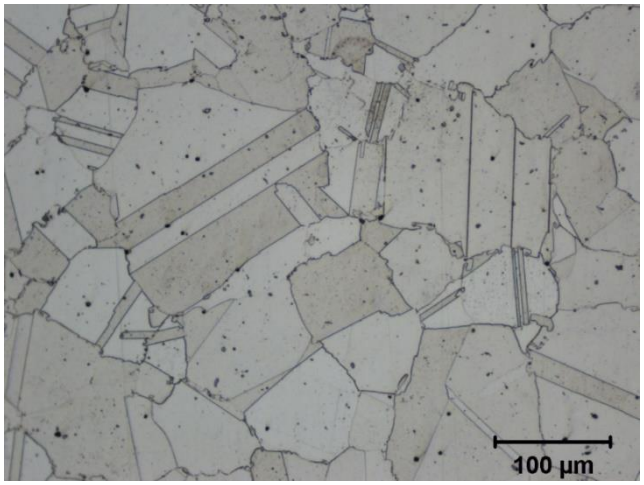

Figure 51. 300H (as heat treated) at 200x magnification

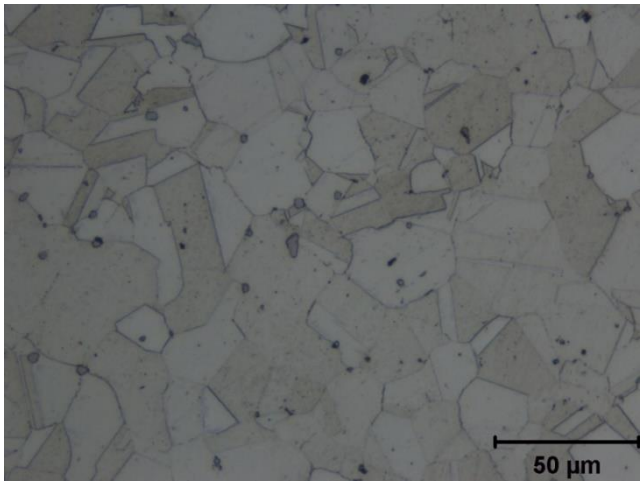

Figure 52. 300 (as received) at 500x magnification

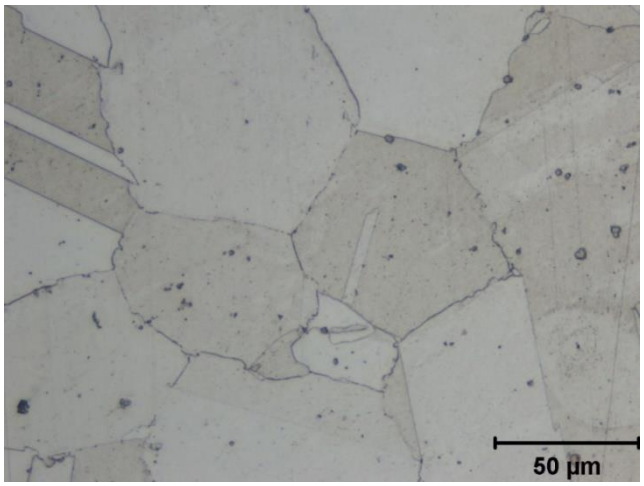

Figure 53. 300H (as heat treated) at 500x magnification

All samples have different microstrure and grain size in their as received condition because of their different chemical composition and production routines. For example, Sample 100 has smaller grain size than the other samples. Gain size is 8-10 µm for Sample 100. This size is 20-25 µm for Sample 200 and 15-20 µm for Sample 300. Finer grain size prevents dislocation motion because it has more grain boundary, and it enhances mechanical properties and hardness. So, this result explains the hardness and tensile test results of as received samples.

Grain size is changed with heat treatment. Grain size is increased for all samples since there is no crystal structure change in the heat treatment. So, there is no recrystallization and grain size increases with heat treatment. In this study, grain size change is shown below.

Grain size sequence in as received condition

Sample 200>Sample 300>Sample100

Grain size sequence in as heat-treated condition

Sample 300>Sample 200>Sample100

After heat treatment, Grain size of Sample 300 is increased more than Sample 200. Incresing in grain size decreases the mechanical properties. These results support the tensile test results.

4.1.5 SEM Analysis Results of Microstructure

Microstructure of all as received and heat-treated samples are analysed by SEM. Moreover, EDS analysis are also performed for samples. First of all, Sample 100 and 100H results are shown in Figure 54, 55 and 56.

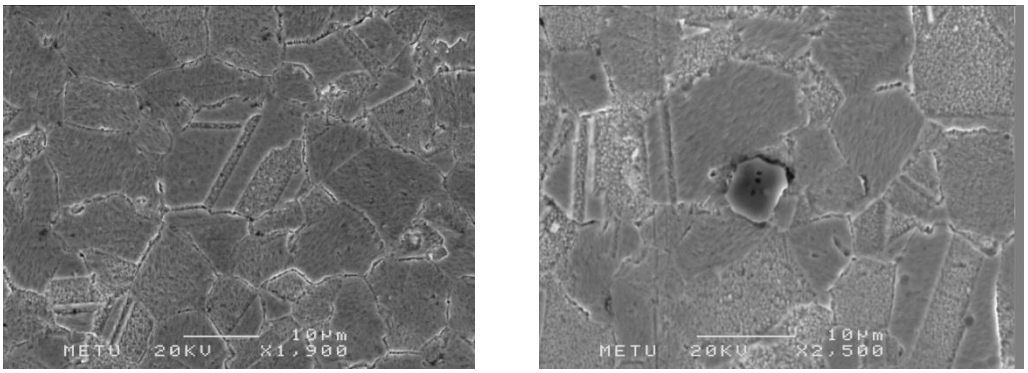

Figure 54. SEM analysis results of 100

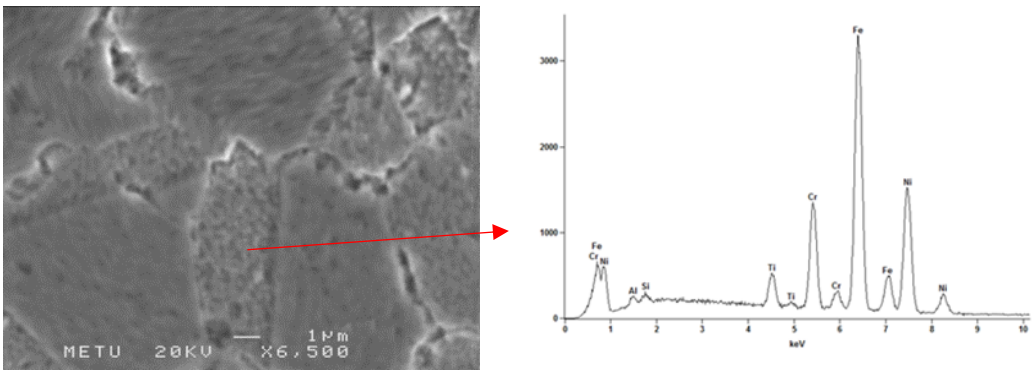

Figure 55. SEM results for 100 at higher magnification and EDS analysis of matrix

In Figure 55, different morphology grains are observed. According to the EDS analysis, all matrix has similar composition.

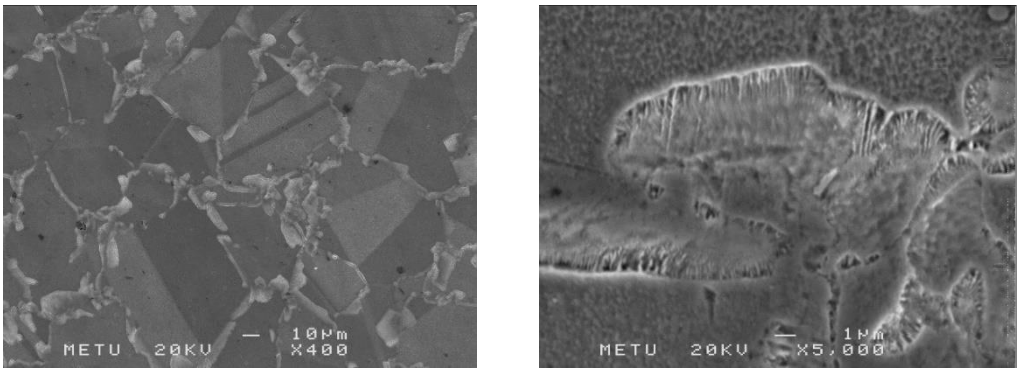

Figure 56. SEM analysis result of 100H general (left) and grain boundary (right) detailed view

In sample 100H, EDS analysis are taken from dark and light matrix, respectively. All results are shown below (Figure 57).

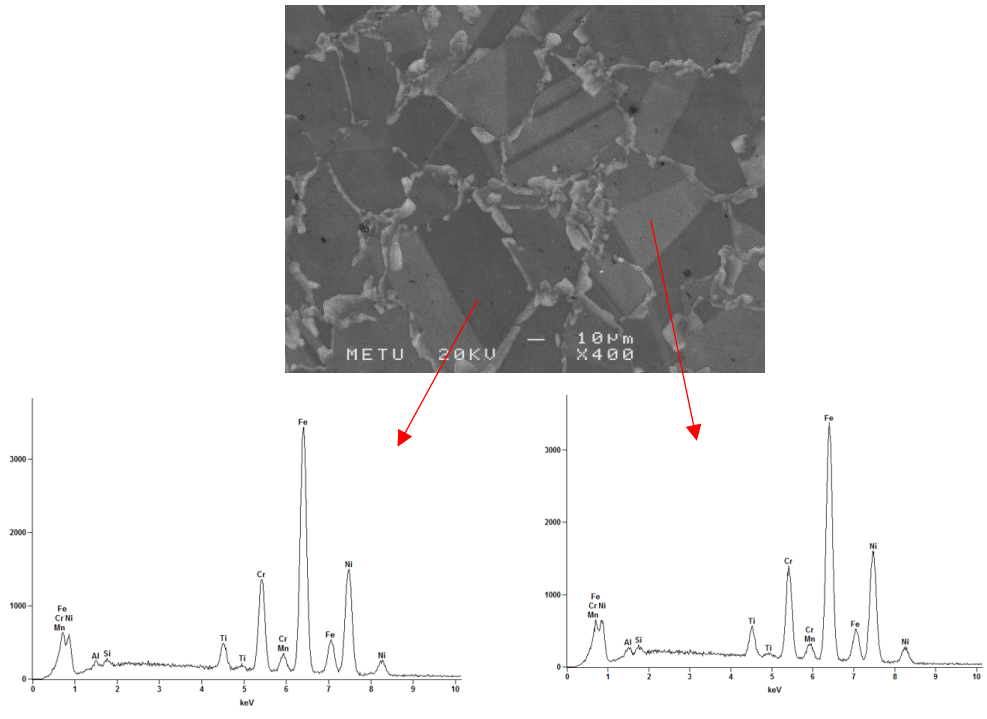

Element	Weight Conc %
Al	0.62
Si	0.37
Ti	2.68
Cr	12.51
Mn	1.08
Fe	49.53
Ni	33.21

Element	Weight Conc %
Al	0.87
Si	0.70
Ti	3.16
Cr	12.15
Mn	1.00
Fe	47.62
Ni	34.50

Figure 57. SEM and EDS analysis result of dark (left) and light (right) matrix of 100H

In addition, different morphology is analysed by EDS (Figure 58).

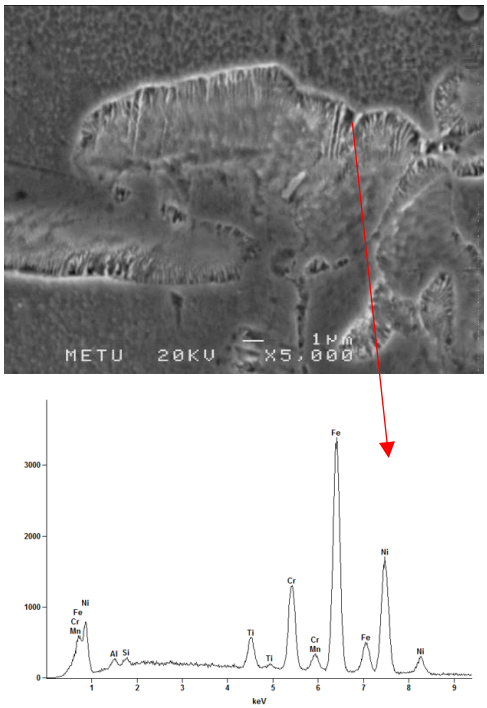

Element	Weight Conc %
Al	0.75
Si	0.48
Ti	3.36
Cr	11.81
Mn	1.04
Fe	46.37
Ni	36.18

Figure 58. SEM and EDS analysis of grain boundary of 100H

Same analysis is done on Sample 200 and Sample 300. The results are represented in Figure 59.

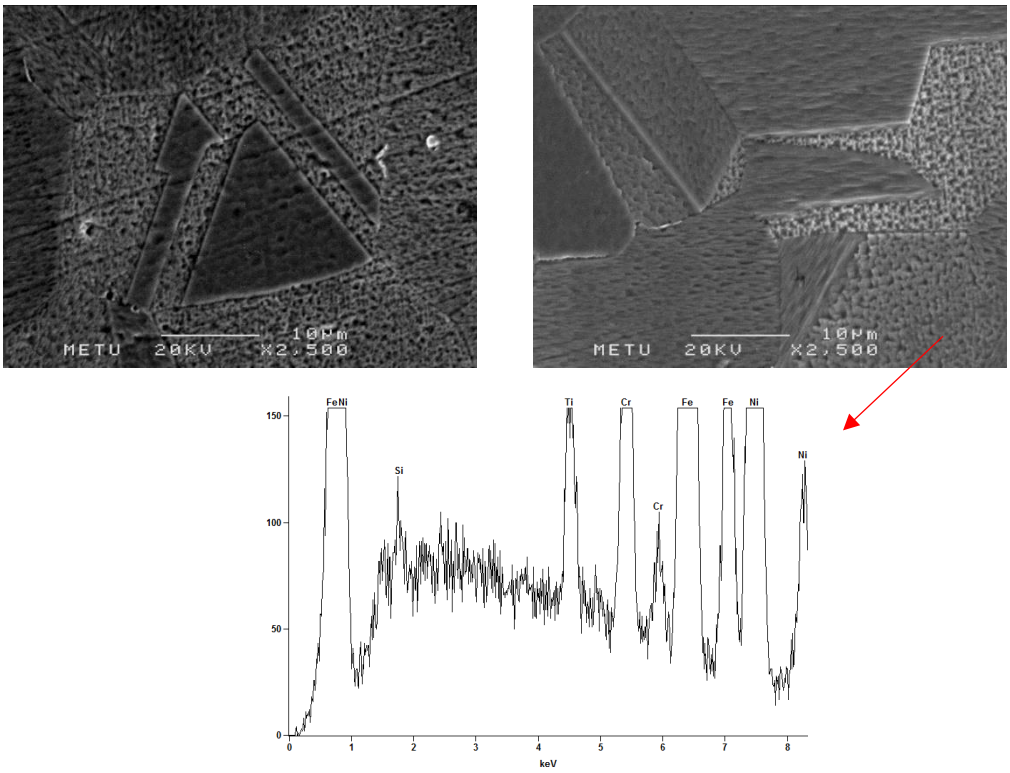

Element	Weight Conc %
Ti	1.96
Cr	6.10
Fe	51.51
Ni	40.43

Figure 59. SEM and EDS analysis of 200

ESD analysis is performed to check grain boundary carbide formation by heat treatment and cubic formation in the structure (Figure 60). In grain boundary there no $Cr_{23}C_6$ formation.

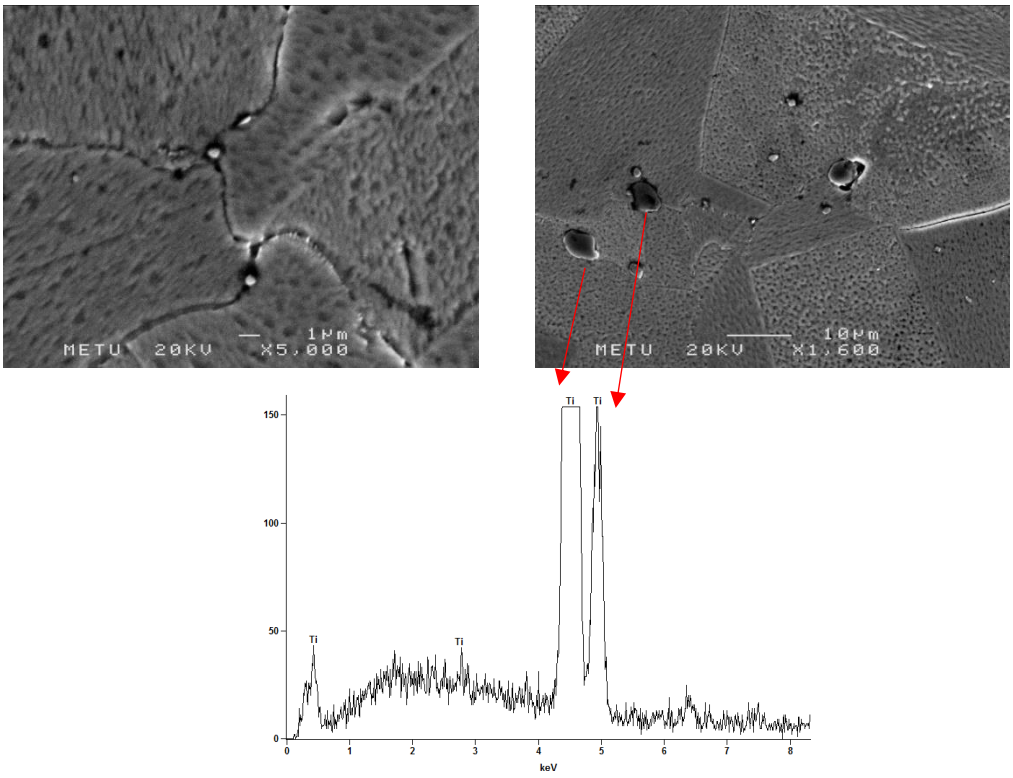

Figure 60. SEM (above) and EDS analysis (below) on cubic particles of 200H

Moreover, cubic structure observed SEM results contains Ti. It can be TiC, TiN or TiCN. C and N are not easily detected wit EDS analsis. Only Ti peaks are seen in the analysis as shown in Figure 60.

JMatPro analysis is studied on three Fe-Ni-based superalloys to support microstructural results. This analysis is used for more information. In JMatPro analysis, CCT and TTT diagram are built. All resutls are shown in Figure 61, 63 and 65, respectively. In addition, phase formation is collected (Figure 62, 64 and 66) with respect to aging time.

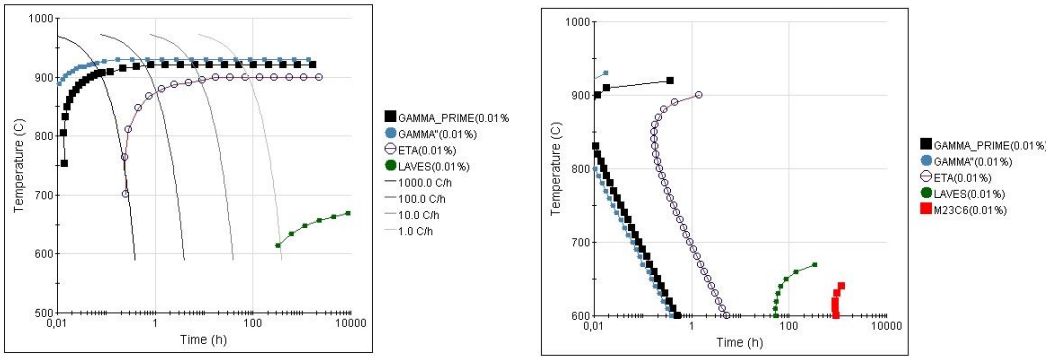

Figure 61. CCT and TTT Diagram for 100 with JMatPro Analysis

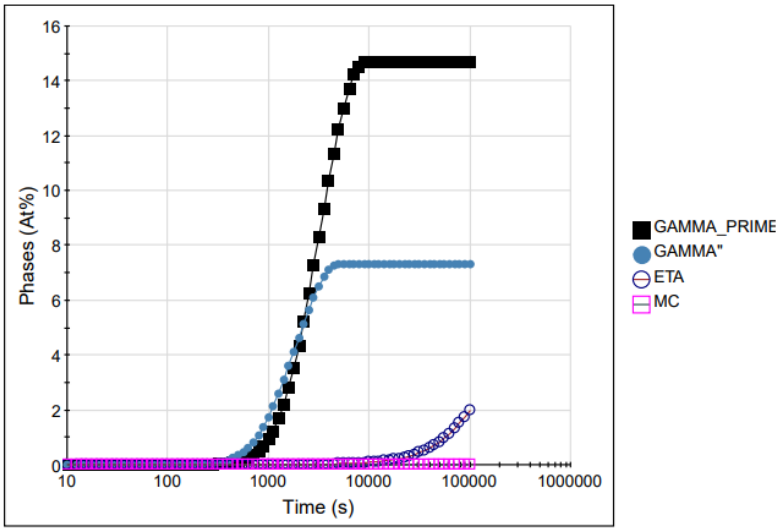

Figure 62. Phase formation after heat treatment for 100

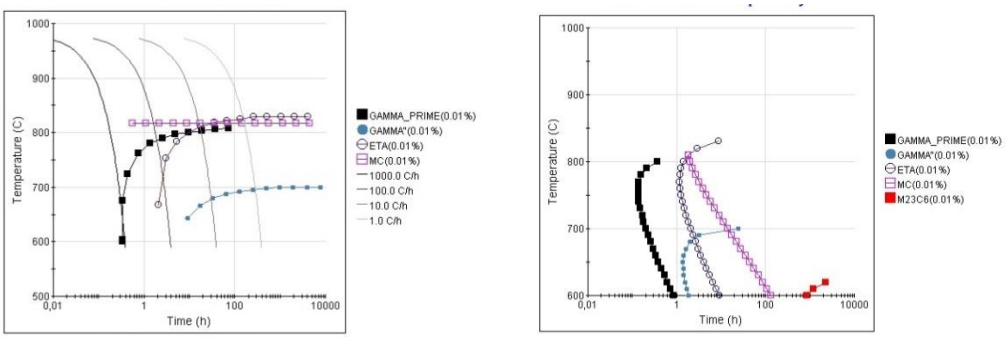

Figure 63. CCT and TTT Diagram for 200 with JMatPro Analysis

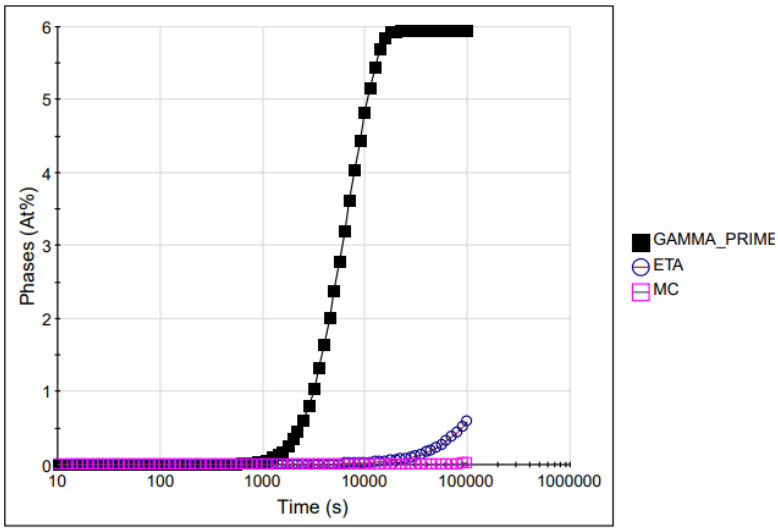

Figure 64. Phase formation after heat treatment for 200

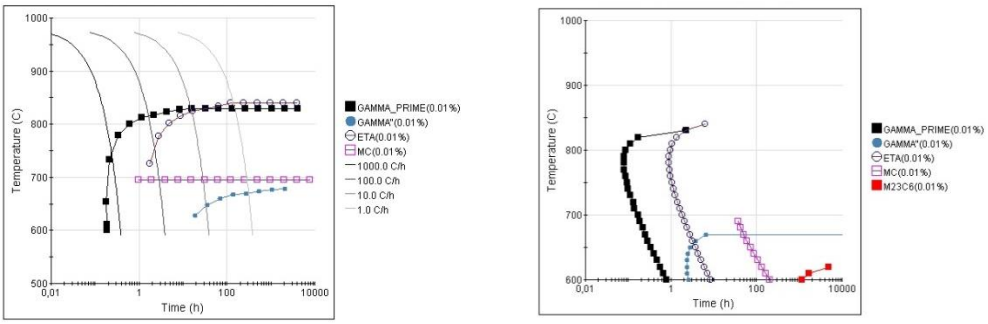

Figure 65. CCT and TTT Diagram for 300 with JMatPro Analysis

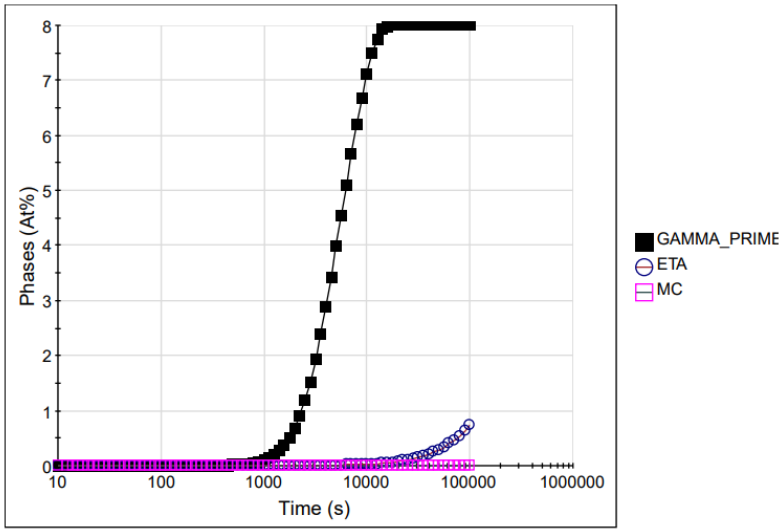

Figure 66. Phase formation after heat treatment for 300

According to the SEM and EDS analysis results, there is no $Cr_{23}C_6$ formation at the grain boundary and in the matrix due to abbreviated time of aging. According to the JMatPro analysis (Figure 61-66) carbide formation is not expected with this heat treatment parameters.

Titanium caride, titanium nitride or tianium carbonitride is observed in the matrix in cubic form. In SEM analysis, spherical γ' can be seen clearly for all samples. Moeover, there are annealing twins in the structure for all samples due to stresses in the structure in the fcc structure. It can be seen that number of twins increase with heat treatment.

Moreover, at the grain boundary of Sample 100, different structure is observed which contain Fe, Ni and Ti. In Figure 62, γ'' formation is observed from analysis. However, in literature, γ'' is generally formed with Nb in Fe-Ni-based superalloys.

4.1.6 Fatigue Crack Growth Test Results

After fatigue crack growth test, crack size (a)- number of cycle (N) graphs are drawn for all samples (Figure 67, 68 and 69).

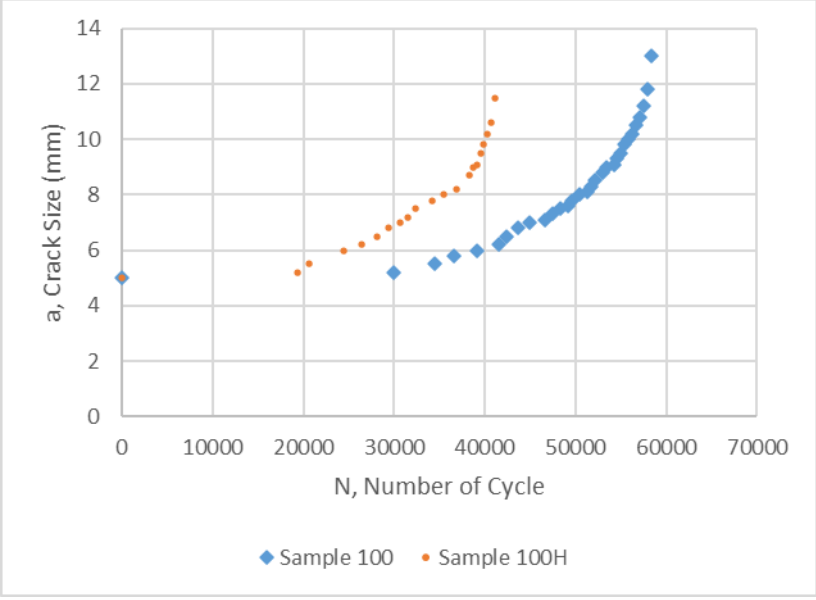

Figure 67. a-N diagram of 100 and 100H

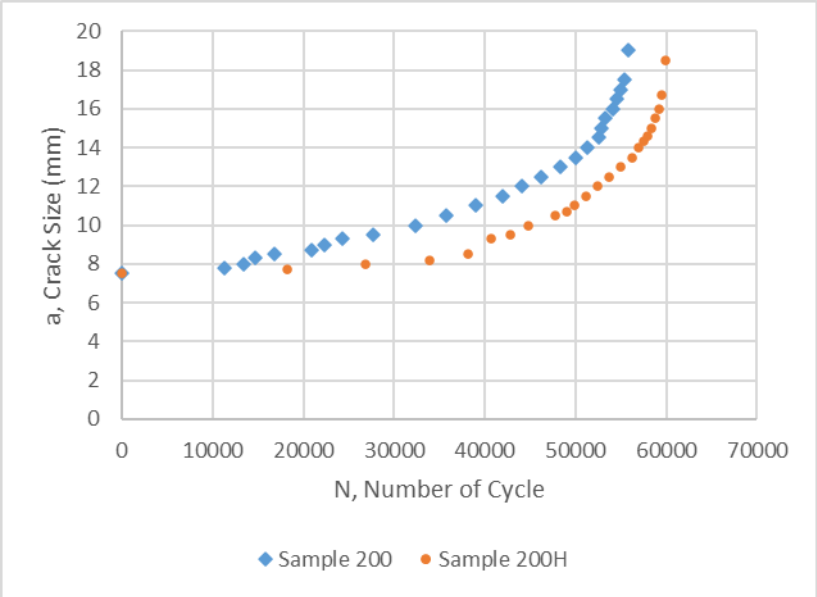

Figure 68. a-N diagram of 200 and 200H

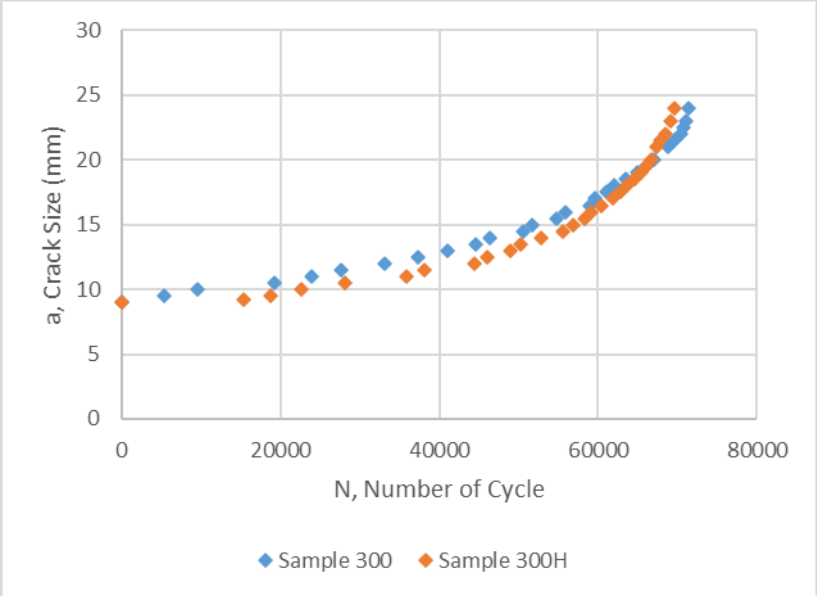

Figure 69. a-N diagram of 300 and 300H

In each sample group, initial crack size is the sam efor as received and as heat treated condition. For example, initial crack size is 5.0 for sample 100 and sample 100H. In sample 200 and 200H, initial crack size is 7.5 mm. This value is 9.0 for Sample 300 and 300H.

Moreover, trend lines are fitted on the al samples to calculate da/dN values. All results are shown in Figure 70, 71 and 72.

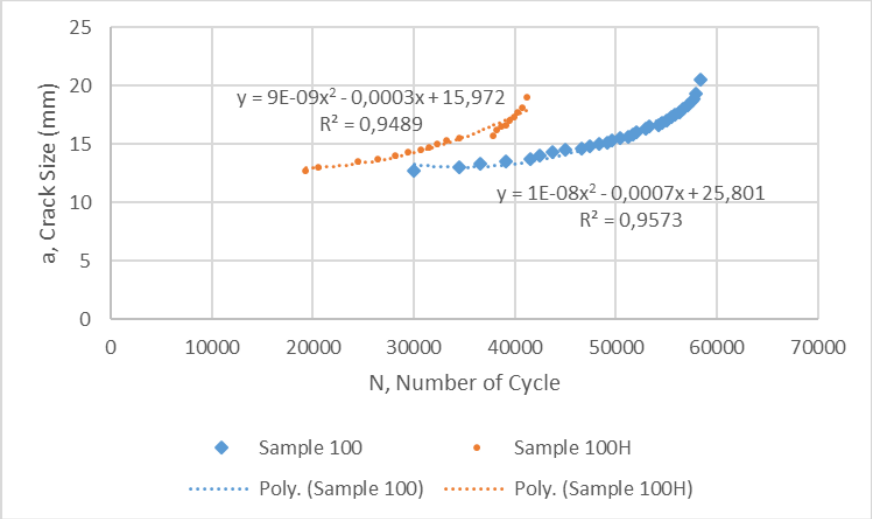

Figure 70. a-N graph with trend line for 100 and 100H

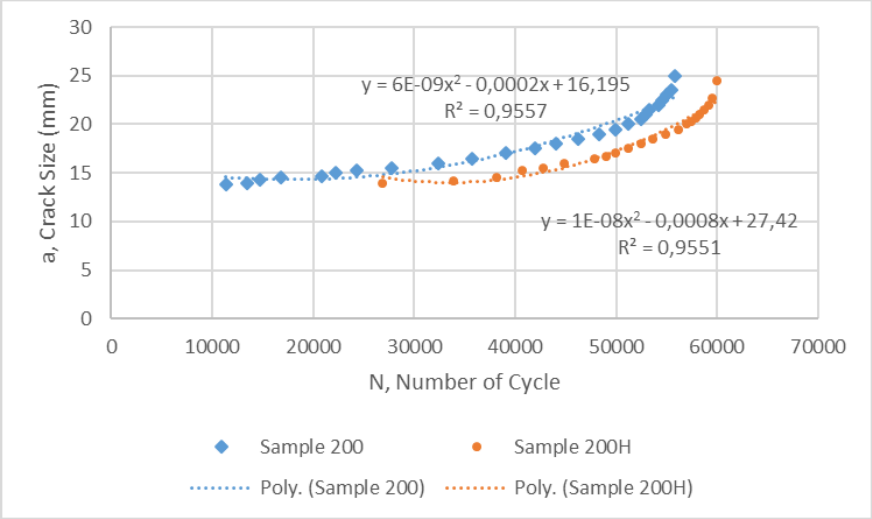

Figure 71. a-N graph with trend line for 200 and 200H

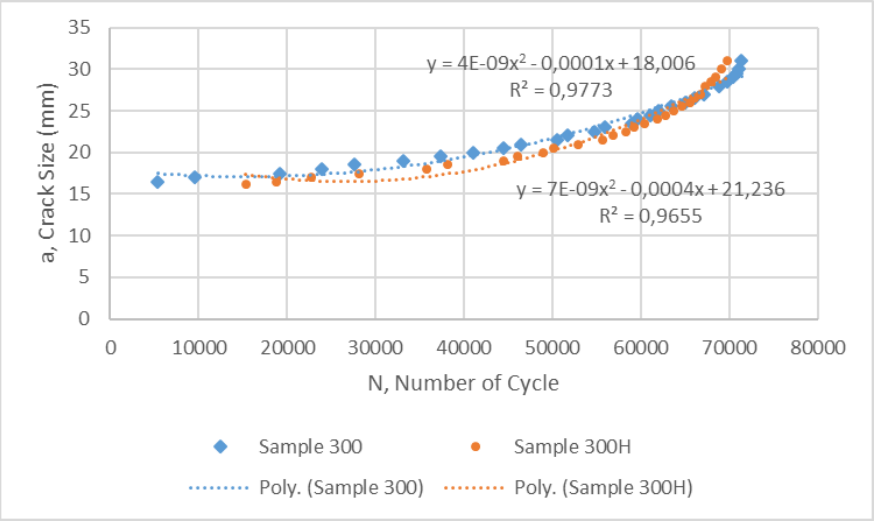

Figure 72. a-N graph with trend line for 300 and 300H

Later, da/dN values are evaluated by seven-point incremental polonomial technique. Moreover, ΔK values are calculated according to fomulas given in below.

$$\Delta K = \frac{\Delta P}{B\sqrt{W}} f(\frac{a}{W})$$

$$\Delta P = \text{Pmax} - \text{Pmin}$$

$$f\left(\frac{a}{W}\right) = \frac{\left(2+\frac{a}{W}\right)[0{,}76 + 4{,}8\frac{a}{W} - 11{,}58\left(\frac{a}{W}\right)^2 + 11{,}43\left(\frac{a}{W}\right)^3 - 4{,}08\left(\frac{a}{W}\right)^4]}{(1-\frac{a}{W})^{3/2}}$$

ΔK: stress intensity factor

P_{max}: maximum load

P_{min}: minimum load

a: crack size

B: thickness of sample

W: width of sample

ΔK-da/dN graphs are shown in below.

Paris-Erdoğan law explains linear part of ΔK versus da/dN graph. The relation formula is shown in below.

$$\frac{da}{dN} = C\Delta K^m$$

According to Paris-Erdoğan law, constant m value can be found from derivative of log (da/dN) versus log ΔK graph (Figure 73-78). Constant C can be calculated by extending the line to intercept log da/dN where ΔK is 1 Mpa√m.

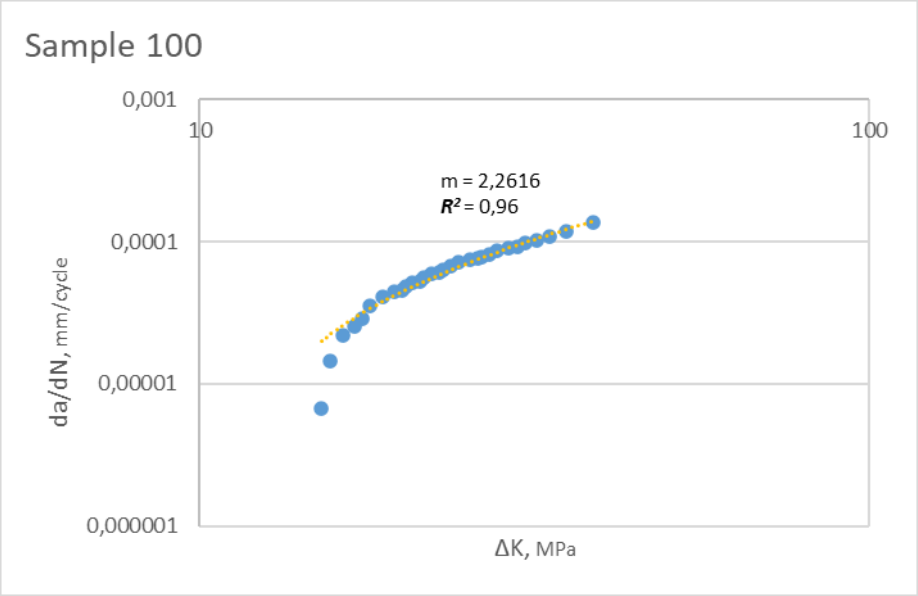

Figure 73. da/dN- ΔK graph of 100

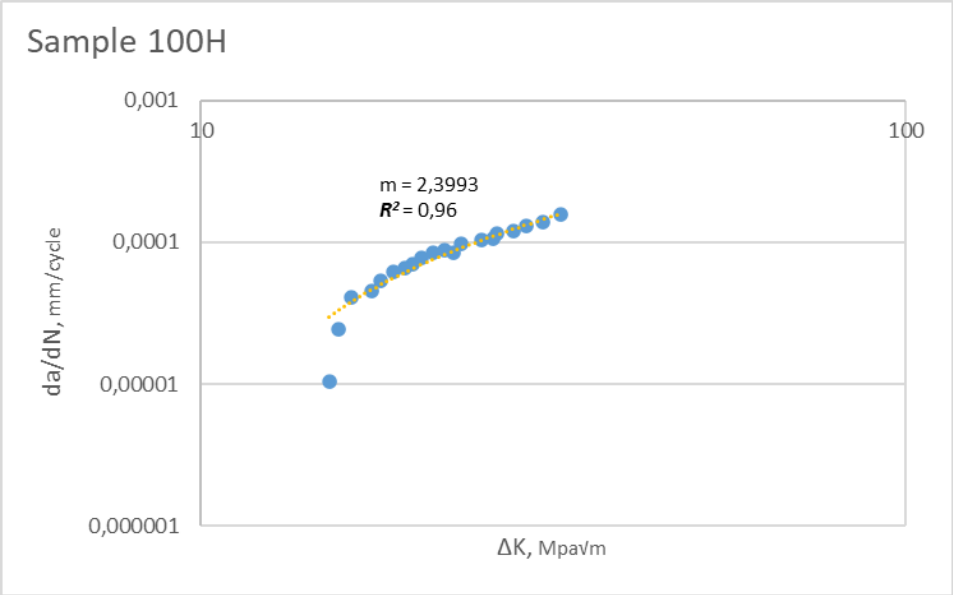

Figure 74. da/dN- ΔK graph of 100H

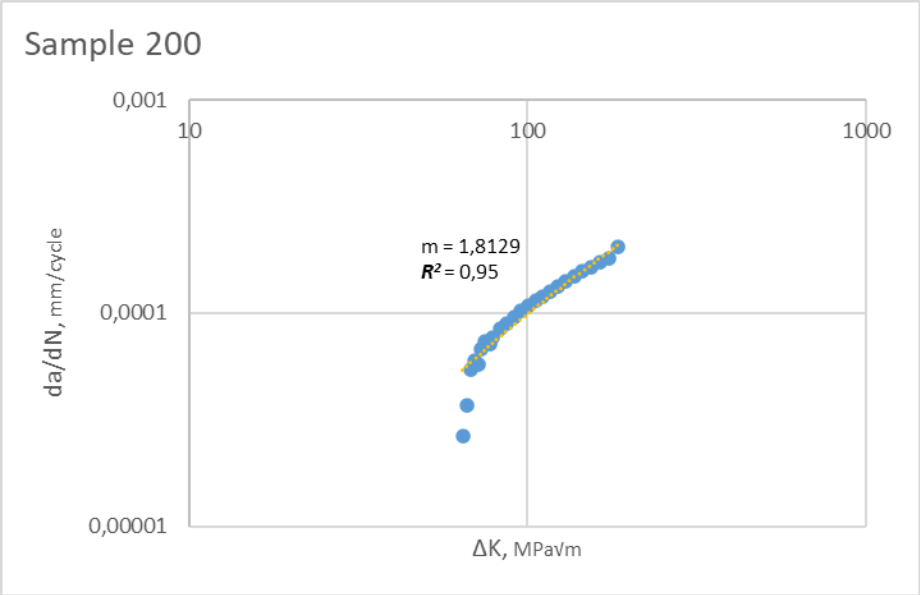

Figure 75. da/dN- ΔK graph of 200

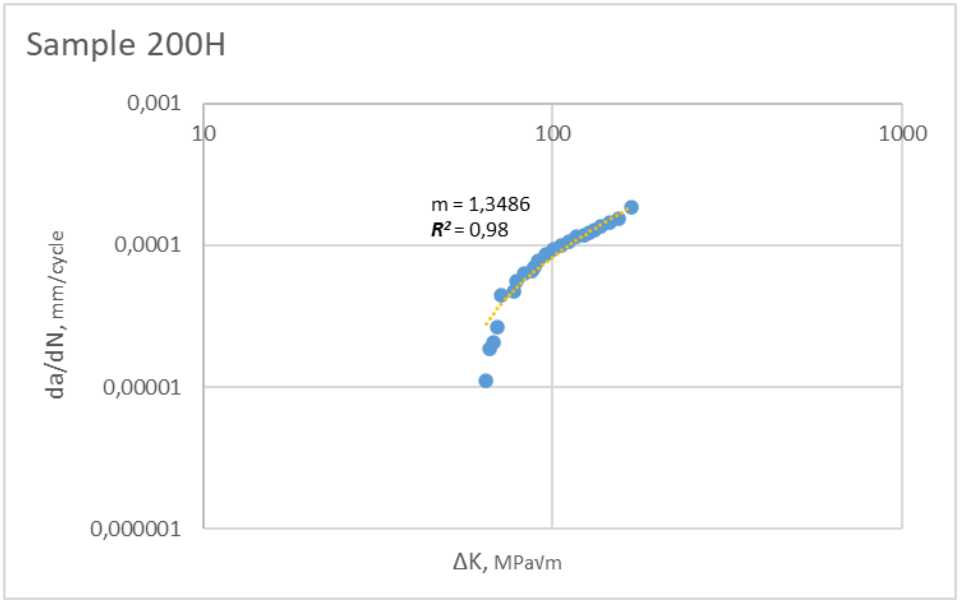

Figure 76. da/dN- ΔK graph of 200H

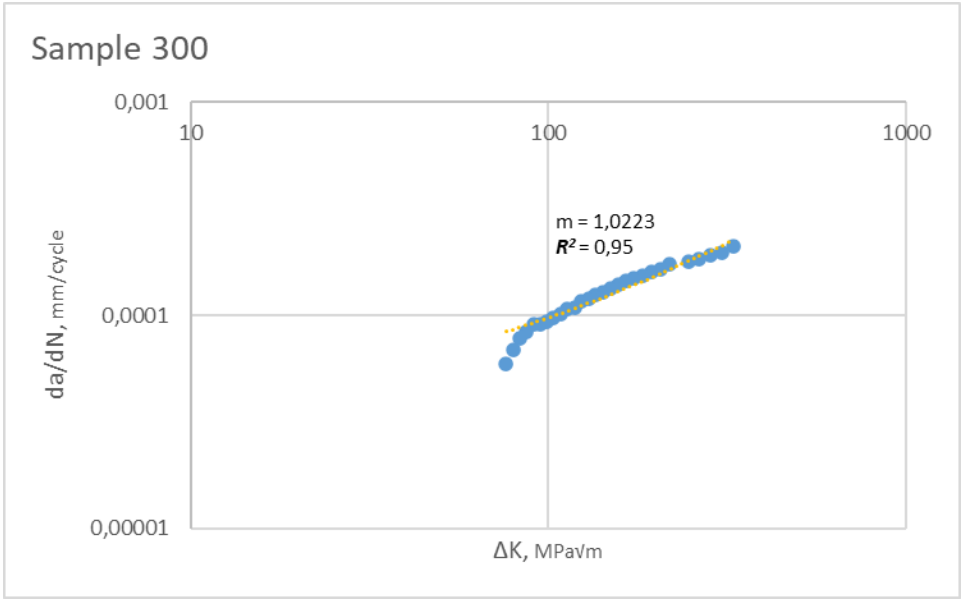

Figure 77. da/dN- ΔK graph of 300

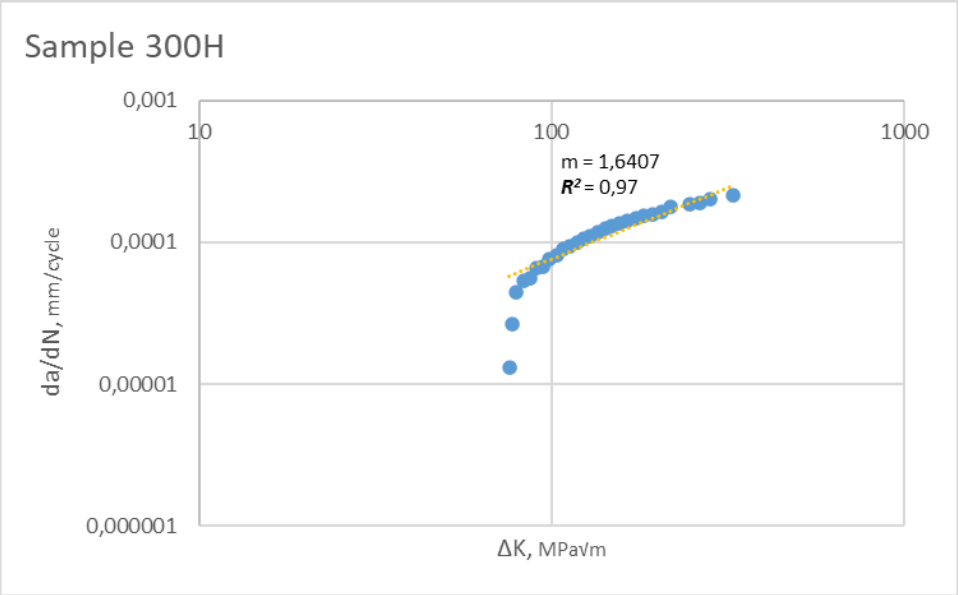

Figure 78. da/dN- ΔK graph of 300H

All results are also summarized at Table 7.

Table 7. m, C, R^2, near ΔKth and ΔKmax values of test samples

Samples	***m***	***C***	***R^2***	***Near ΔK_{th} (MPa√m)***	***ΔK_{max} (MPa√m)***
Sample 100	2.2616	5.061*10^-8	0.9562	15	40
Sample 100H	2.3993	5.140*10^-8	0.9633	15	35
Sample 200	1.8129	2.716*10^-8	0.9520	64	130
Sample 200H	1.3486	1.794*10^-7	0.9850	68	180
Sample 300	1.0223	8.980*10^-7	0.9485	72	200
Sample 300H	1.6407	3.835*10^-8	0.9695	70	180

In addition, da/dN-ΔK graphs are drawn for as received and heat treated for each group (Figure 79, 80 and 81).

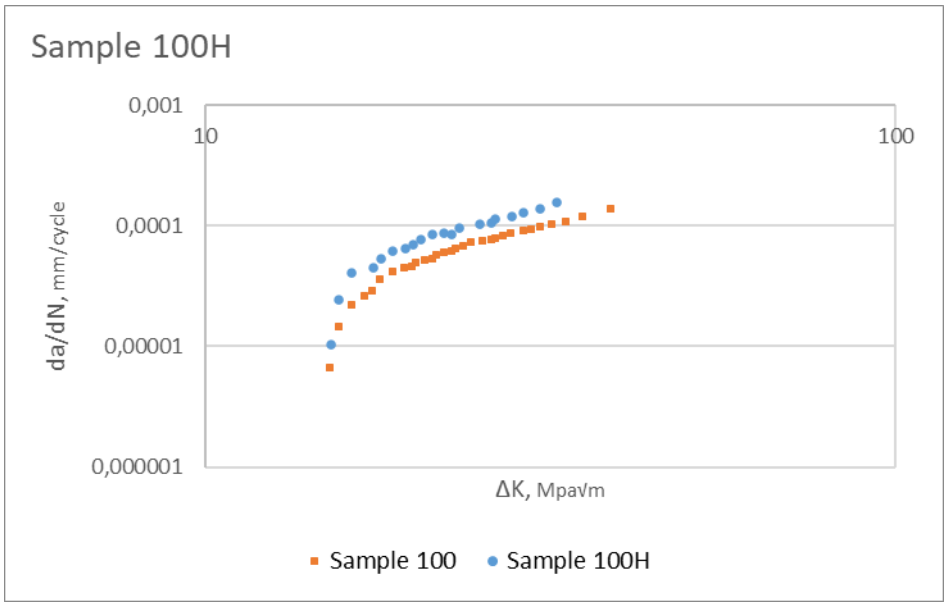

Figure 79. da/dN- ΔK graph of 100 and 100H

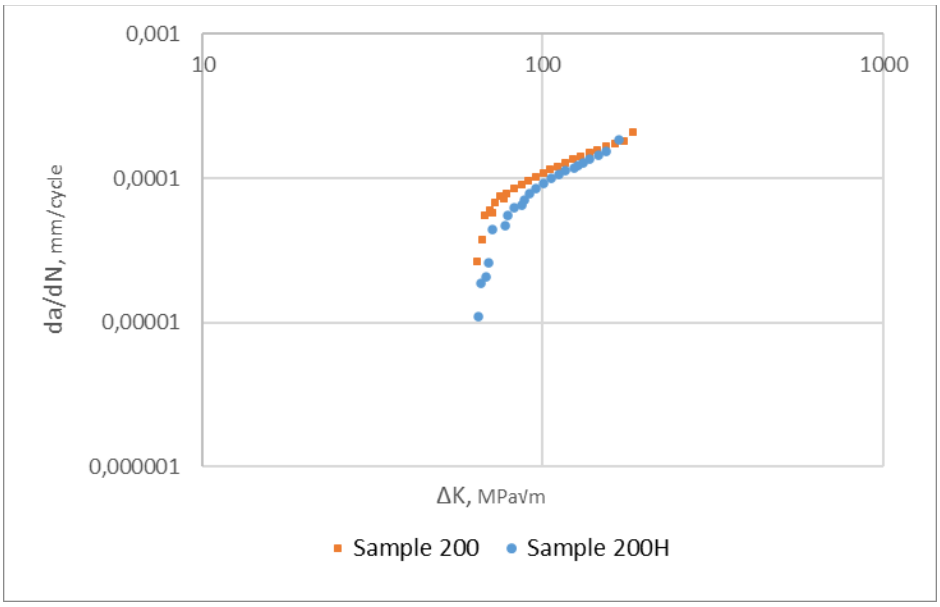

Figure 80. da/dN- ΔK graph of 200 and 200H

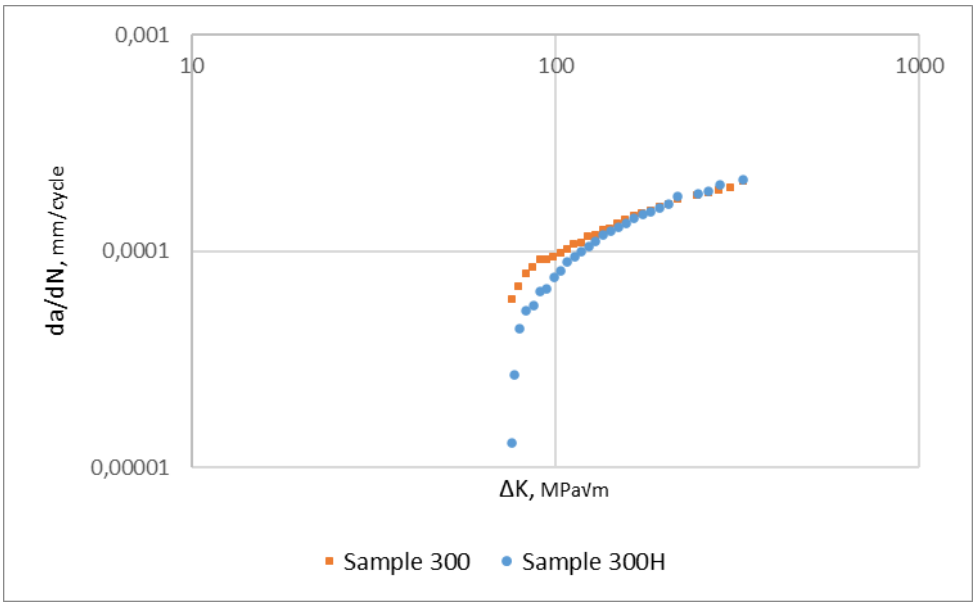

Figure 81. da/dN- ΔK graph of 300 and 300H

According to the fatigue crack growth results, crack growth rate is ascended with heat treatment for Sample 100 and Sample 300. It means that heat treatment does not improve the crack growth performance. Actually, there are slight differences between as received and as heat treated condition like other test results. The crack growth rate is declined in Sample 200 after heat treatment. These results support the other results. In Table 7, m values are listed. If m value is increased, da/dN values are also increase. m values of Sample 100 and Sample 300 are increased with heat treatment. On the contrary, m valus of Sample 200 is reduced. So, crack growth rate is declined with heat treatment in this sample. In comparision, it can be said that heat treatment parameter is the best parameter for Sample 200.

According to the da/dN-ΔK results, maximum ΔK_{max} valuesare calculated. This value close to fracture toughness value for a given thickness value of the samples. For example, ΔK_{max} values are 40 MPa√m for Sample 100 and 35 MPa√m for Sample 100H. In sample 200, fracture toughness value is 130 MPa√m while this value is 180 MPa√m for Sample 200H. Finally, fracuture toughness of Sample 300 200 MPa√m and 180 MPa√m for sample 300H. The results support the m values. The grain size of Sample 100 and 100H is lower than other samples. In microstructure, different

morpholojic structure is observed. It can be reduced grain boundary strengthening so crack growth rate is higher than others. Diffrence between sample 200 and 300 can be came from thickness differences of them. In conclusion, fracture toughness of Sample 200 is improved by heat treatment and all results support this value.

4.1.7 Fractographic Results

Fractography is studied on tensile and fatigue crack growth fracture surface, respectively.

4.1.7.1 Fractographic Results of Tensile Test Samples

The first results are collected from tensile test specimens. All results are shown in Figure 82-85.

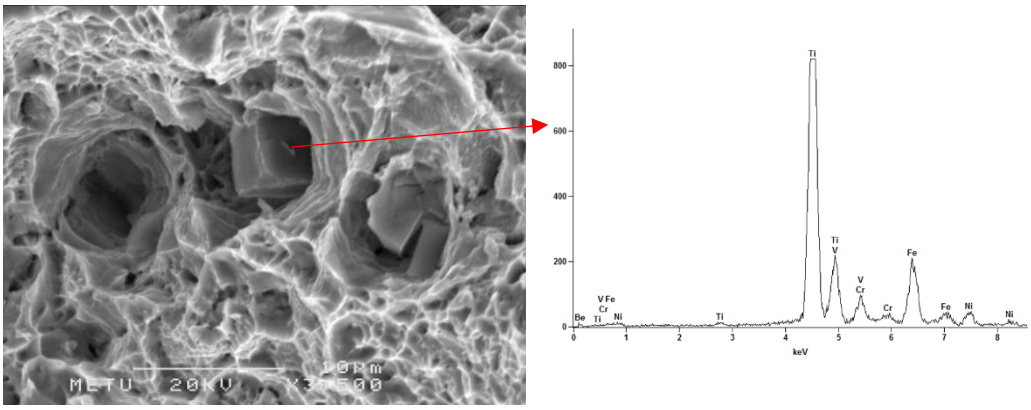

Figure 82. Tensile fracture surface of 100 at SEM and EDS analysis of cubic particle

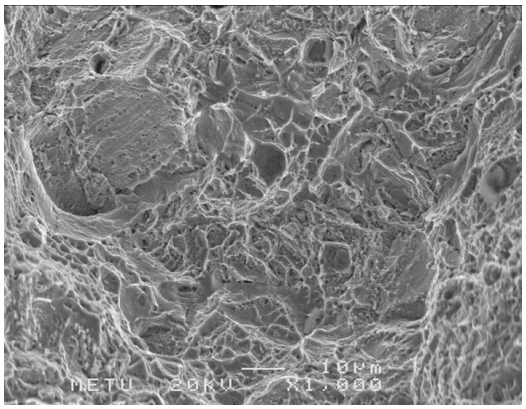

Figure 83.Tensile fracture surface of 100H at SEM

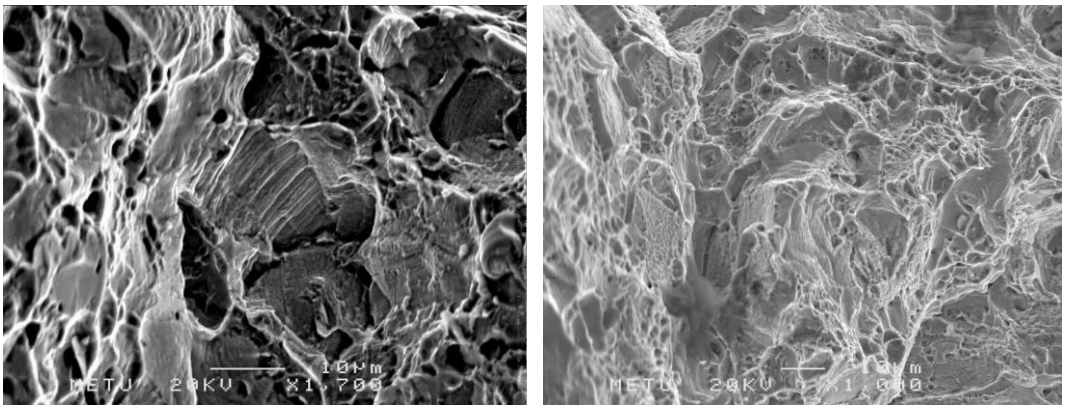

Figure 84. Tensile fracture surface of 200 (left) and 200H (right) at SEM

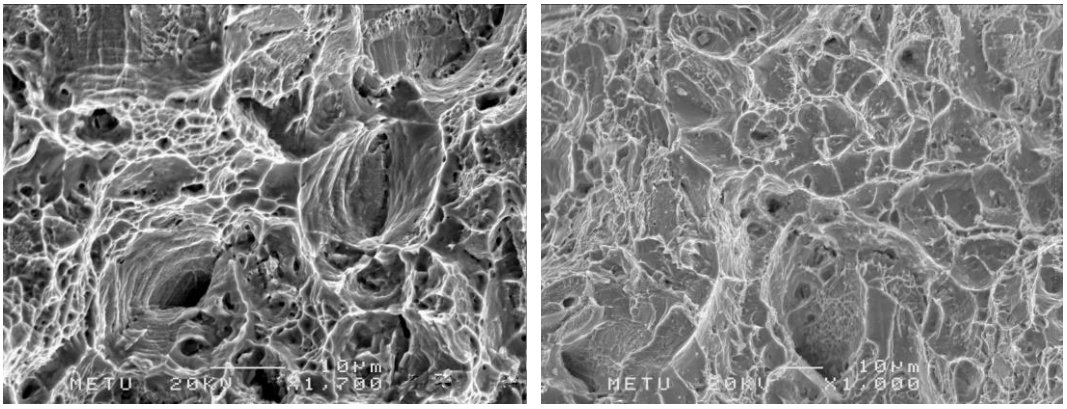

Figure 85. Tensile fracture surface of 300 (left) and 300H (right) at SEM

According to the results, three samples possess ductile behaviour. On tensile test specimen surface, dimples can be seen clearly. After heat treatment, more brittle regions also exist but general trend is ductile for all samples.

4.1.7.2 Fractographic Results of Fatigue crack growth Test Samples

Fractographic results are also performed for fatigue crack growth samples. Macro and micro fractographic results are shown in Figure 86-94.

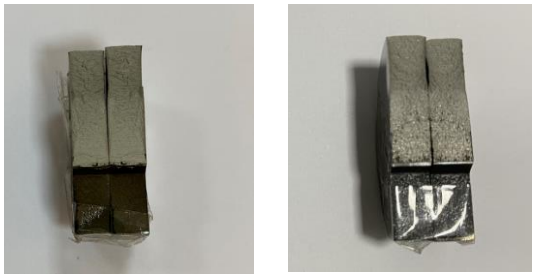

Figure 86. Fracture surface of 100 and 100H

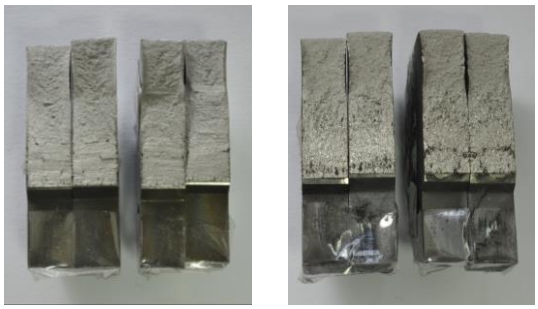

Figure 87. Fracture surface of 200 and 200H

Figure 88. Fracture surface of 200 and 200H

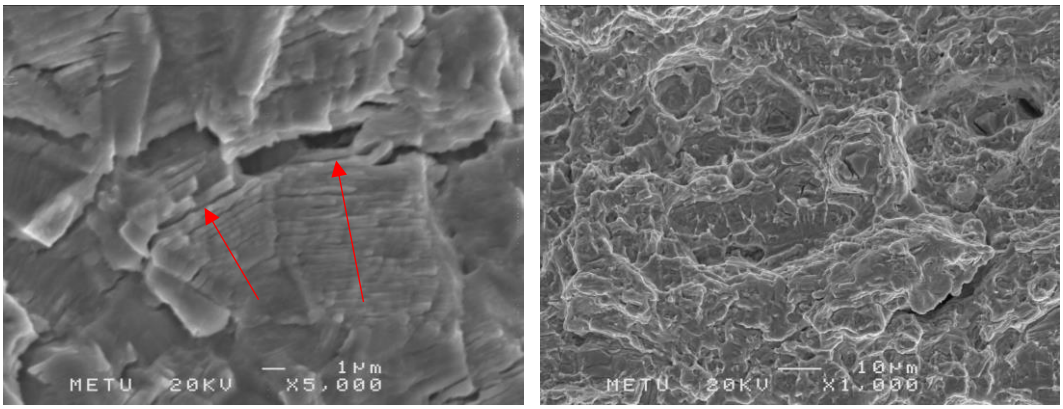

Figure 89. Fatigue crack growth (left) and fast fracture region (right) of 100

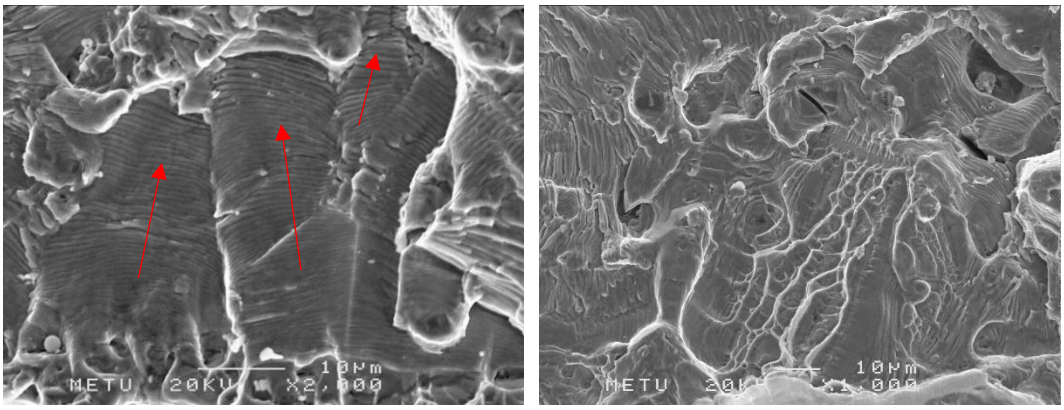

Figure 90. Fatigue crack growth (left) and fast fracture region (right) of 100H

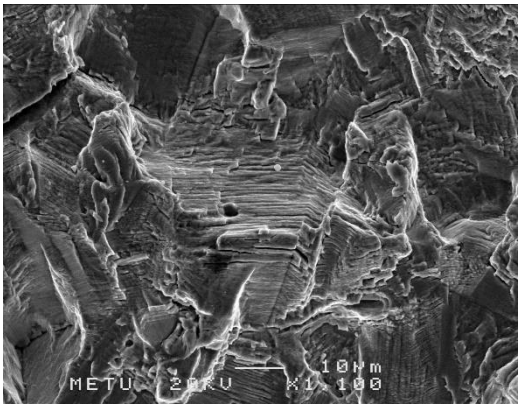

Figure 91. Fatigue crack growth region of 200

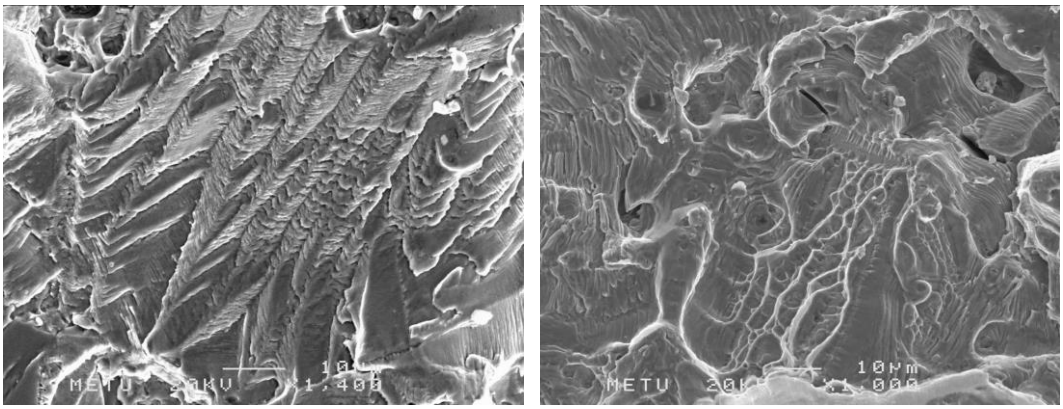

Figure 92. Fatigue crack growth (left) and fast fracture region (right) of 200H

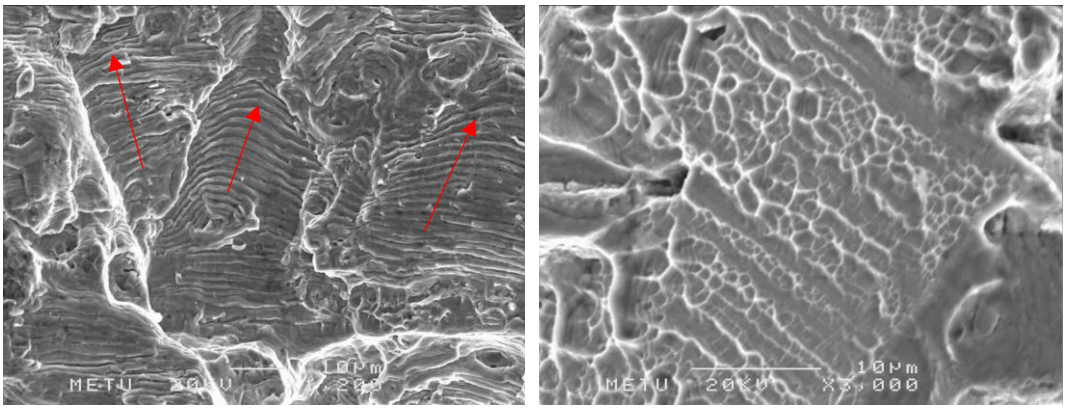

Figure 93. Fatigue crack growth (lef) and fast fracture region (right) of 300

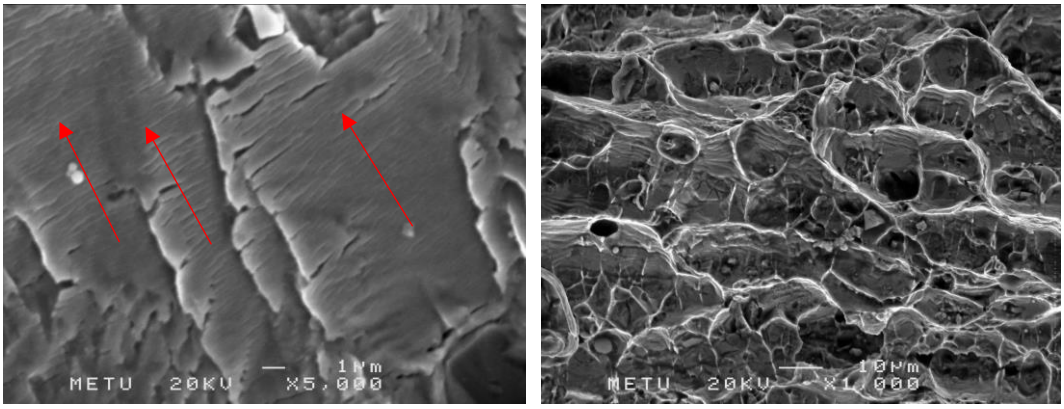

Figure 94. Fatigue crack growth (left) and fast fracture (right) region of 300H

According to the crack growth fractographic results, all samples have similar aspects. In crack growth region, striations, secondary cracks, and slip bands are observed. In fast fracture region, dimples can be seen. These results support the tensile test

fracture surface. These three materials behave ductile material. In generally, crack growth direction is north for SEM results are shown above.

CHAPTER 5

CONCLUSION

In this study, precipitation of γ' which is the main strengthening mechanism of Fe-Ni-based superalloys, is observed for all samples. However, there is no carbide precipitation at the grain boundary and in the matrix due to short aging time. Heat treatment can be conducted with prolonged aging time to observe carbide precipitation and its effect on characterization and mechanical properties. Moreover, Aging temperature can be decreased to reduced grain growth rate and its effects on chracaterization and mechanical properties can be also discussed.

It is observed that characterization and mechanical properties of three different Fe-Ni-based superalloys possess different response against same heat treatment parameters. According to the results, heat treatment parameter, which is applied in this study, is the best parameter for Sample 200. On the contrary, this heat treatment is the worst parameter for Sample 300.

Even though Sample 200 and Sample 300 have similar production routes, their response to heat treatment are different from each other. Grain growth is higher in Sample 300 than in 200 due to a slight difference in chemical composition. So, mechanical properties are reduced in Sample 300.

In this study, there is no effect of heat treatment on Sample 100. The reason of that can be different chemical composition and production routine of Sample 100. Different temperature and time parameters can be applied on this Sample to see heat treatment's effect on characterization and mechanical properties of this sample.

According to the fatigue crack growth results, this heat treatment parameter is the best parameter for Sample 200. In sample 300, crack growth rate is increased with heat treatment due to higher grain growth in Sample 300 than Sample 200. In sample

100, crack growth performance is not improved with heat treatment. As with other test results, fatigue crack growth results are not changed drastically with heat treatment.

In this study, all results support each other for as received and heat-treated samples.

REFERENCES

[1] J. R. Davis, Dü., Heat-resistant Materials, ASM International, 1997.

[2] M. J. Donachie ve S. J. Donachie, Superalloys A Technical Guide, ASM International, 2002.

[3] B. Geddes, H. Leon ve X. Huang, Superalloys Alloying and Performance, ASM International, 2010.

[4] A. Günen, M. Keddam, S. Alkan, A. Erdoğan ve M. Çetin, «Microstructural characterization, boriding kinetics and tribo-wear behavior of borided Fe-based A286 superalloy,» *Materials Characterization,* cilt 186, pp. 1-19, 2022.

[5] J. Ridhwan, E. Hamzah, H. Effendy, M. Selamat ve Z. Zulfattah, «Effect of Cooling Rate on The Microstructures And Hardness Of Fe-Ni-Cr Superalloy,» *Journal of Mechanical Engineering and Technology,* cilt 5, no. 1, pp. 45-57, 2013.

[6] X. Zhao, Y. Dang, H. Yin, J. Lu, Y. Yuan, Z. Yang ve J. Yan, «Effect of heat treatment on the microstructure of a Ni–Fe based superalloy for advanced ultra-supercritical power plant applications,» *Progress in Natural Science: Materials International,* cilt 26, pp. 204-209, 2016.

[7] R. C. Reed, The Superalloys Fundamentals and Applications, Cambridge: Cambridge University Press, 2006.

[8] O. Takakuwa, Y. Ogawa, J. Yamabe ve H. Matsunaga, «Hydrogen-induced ductility loss of precipitation-strengthened Fe-Ni-Cr based superalloy,» *Materials Science & Engineering A,* cilt 739, pp. 335-342, 2019.

[9] Z. Zhao, P. Zhang, S. Li, J. Zhang, W. Shi, C. Zhang, Y. Li, J. Yan, F. Yang ve C. Zhang, «Fatigue-creep behaviors of NieFe based superalloy under

various testing conditions,» *journal of materials research and technology,* cilt 15, pp. 4694-4701, 2021.

[10] N. V. Kazantseva, N. N. Stepanova ve M. B. Rigmant, Superalloys Analysis and Control of Failure Process, CRC Press, 2019.

[11] Ó. Martín, P. D. Tiedra ve M. San-Juan, «Combined effect of resistance spot welding and precipitation hardening on tensile shear load bearing capacity of A286 superalloy,» *Materials Science & Engineering A,* pp. 309-314, 2017.

[12] J. Ridhwan, E. Hamzah, M. Selamat, Z. Zulfattah ve M. Hafidzal, «EFFECT OF AGING TREATMENT ON THE MICROSTRUCTURES AND HARDNESS OF Fe-Ni-Cr SUPERALLOY,» *International Journal of Automotive and Mechanical Engineering,* no. 8, pp. 1430-1441, 2013.

[13] K. VATTAPPARA, «Understanding the effect of temperature and time on Gamma prime coarsening for Nickel-base superalloy Haynes 282,» KTH Royal Institute of Technology, Stockholm, 2019.

[14] G. V. Shlyakhova, A. V. Bochkareva ve M. V. Nadezhkin, «EFFECT OF HEAT TREATEMEMT ON MICROSTRUCTURE AND MECHANICAL PROPERTIES OF THE PRECIPITATION HARDENING ELINVAR ALLOY,» *Russian Physics Journal,* cilt 64, no. 5, pp. 838-843, 2021.

[15] R. Viswanathan ve J. Nutting, Advanced Heat Resistant Steels for Power Generation, London: IOM Communication, 1999.

[16] B. B. Zhang, F. K. Yan, M. J. Zhao, N. R. Tao ve K. Lu, «Combined strengthening from nanotwins and nanoprecipitates in an iron-based superalloy,» *Acta Materialia,* pp. 310-320, 9 April 2018.

[17] D. Raynor ve J. M. Silcock, «Strengthening Mechanism in y' Precipitating Alloys,» *Metal Science Journal,* pp. 121-130, 2 January 1970.

[18] Y. Yan, Y. Yan, Y. He, J. Li, Y. Su ve L. Qiao, «The mechanism of precipitation strengthening in Fe–Ni austenitic alloy electron beam weldment,» *Materials Science & Engineering A,* pp. 85-89, 6 February 2015.

[19] K. Lu, F. K. Yan, H. T. Wang ve N. R. Tao, «Strengthening austenitic steels by using nanotwinned austenitic grains,» *Scripta Materialia,* pp. 878-883, 5 January 2012.

[20] A. B. Jacuinde, L. Arias ve B. Hernandez, «Kinetics of Secondary Carbides Precipitation in a High-Chromium White Iron,» *Journal of Materials Engineering and Performance,* pp. 371-382, 2003.

[21] R. Jumaidin, E. Hamzah, H. Effendy, M. Z. Selamat ve Z. Zulfattah, «Effect of Cooling Rate on The Microstructures and Hardnessof Fe-Ni-Cr Superalloy,» *International Journal of Automotive and Mechanical Engineering* , pp. 1430-1441, July 2013.

[22] X. F. Wang, «Effects of High Temperature and Cryogenic Treatment on The Microstructure and Abrasion Resistance of a High Chromium Cast Iron,» *Journal of Materials Processing Technology,* pp. 3236-3240, 2009.

[23] W. D. Callister Jr. ve D. G. Rethwisch, Fundamentals of Materials Science and Engineering, Wiley, 2001.

[24] H. A. Richard ve M. Sander, Fatigue Crack Growth, Springer Cham, 2016.

[25] R. W. Hertzberg, R. P. Vinci ve J. L. Hertberg, Deformation and Fracture Mechanics of Engineering Materials, Haboken: John Wiley & Sons, Inc, 2012.

[26] L. M. Tudose ve O. C. Popa, «Stress Intensity Factors Analysis on Cracks in the Hertzian Stresses Field of Teeth Gears,» %1 içinde *The 10th International Conference on Tribology "ROTRIB'07"*, Bucharest, 2007.

[27] F. Ellyin, Fatigue Damage, Crack Growth and Life Prediction, Springer Science & Business Media, 2012.

[28] *ASTM E8/E8M-21 Standard Test Methods for Tension Testing of Metallic Materials*, ASTM International.

[29] *ASTM E399-22 Standard Test Method for Linear-Elastic Plane-Strain Fracture Toughness of Metallic Materials*, ASTM International.

[30] S. Suresh, Fatigue of materials, Cambridge University Press, 1998.